Sodium perturbs mitochondrial respiration and induces dysfunctional Tregs

Peer-reviewed author version

FERNANDES CORTE-REAL, Beatriz; HAMAD, Ibrahim; ARROYO HORNERO, Rebeca; Geisberger, Sabrina; Roels, Joris; VAN ZEEBROECK, Lauren; DYCZKO, Aleksandra; van Gisbergen, Marike W.; Kurniawan, Henry; Wagner, Allon; Yoset, Nir; Weiss, Susanne N. Y.; Schmetterer, Klaus G.; Schroeder, Agnes; Krampert, Luka; Haase, Stefanie; Bartolomaeus, Hendrik; HELLINGS, Niels; Saeys, Yvan; Dubois, Ludwig J.; Brenner, Dirk; Kempa, Stefan; Hafler, David A.; Stegbauer, Johannes; Linker, Ralf A.; Jantsch, Jonathan; Mueller, Dominik N. & KLEINEWIETFELD, Markus (2023) Sodium perturbs mitochondrial respiration and induces dysfunctional Tregs. In: Cell Metabolism, 35 (2) , p. 299 - 315.

DOI: 10.1016/j.cmet.2023.01.009
Handle: http://hdl.handle.net/1942/40896

Sodium perturbs mitochondrial respiration and induces dysfunctional Tregs

Beatriz F. Côrte-Real[1,2,†], Ibrahim Hamad[1,2,†], Rebeca Arroyo Hornero[1,2], Sabrina Geisberger[3,4,5,6], Joris Roels[7,8], Lauren Van Zeebroeck[1,2], Aleksandra Dyczko[1,2], Marike W. van Gisbergen[9], Henry Kurniawan[10], Allon Wagner[11,12], Nir Yosef[11,12,13,14,15], Susanne N.Y. Weiss[16], Klaus G. Schmetterer[16,17], Agnes Schröder[18], Luka Krampert[16], Stefanie Haase[19], Hendrik Bartolomaeus[3,5], Niels Hellings[2], Yvan Saeys[7], Ludwig J. Dubois[9], Dirk Brenner[10,20], Stefan Kempa[4], David A. Hafler[21,22], Johannes Stegbauer[23], Ralf A. Linker[19], Jonathan Jantsch[16,24], Dominik N. Müller[3,5,6,25,#], Markus Kleinewietfeld[1,2,#,*]

Affiliations

[1] VIB Laboratory of Translational Immunomodulation, VIB Center for Inflammation Research (IRC), Hasselt University, 3590 Diepenbeek, Belgium

[2] Department of Immunology, Biomedical Research Institute, Hasselt University, 3590 Diepenbeek, Belgium

[3] Experimental and Clinical Research Center, a joint cooperation of Max Delbrück Center for Molecular Medicine and Charité-Universitätsmedizin Berlin, 13125 Berlin, Germany

[4] Max-Delbrück-Center for Molecular Medicine in the Helmholtz Association (MDC), Berlin Institute for Medical Systems Biology (BIMSB), Integrative Proteomics and Metabolomics, 13125 Berlin, Germany

[5] DZHK (German Centre for Cardiovascular Research), partner site Berlin, 10785 Berlin Germany

[6] Charité – Universitätsmedizin Berlin, Corporate Member of Freie Universität Berlin, Humboldt Universität zu Berlin, and Berlin Institute of Health, 10117 Berlin, Germany

[7] VIB-UGent Center for Inflammation Research, 9052 Gent, Belgium

[8] VIB BioImaging Core, 9052 Gent, Belgium

[9] The M-Lab, Department of Precision Medicine, GROW – School for Oncology and Developmental Biology, Maastricht University, 6200 MD Maastricht, The Netherlands

[10] Experimental & Molecular Immunology, Department of Infection and Immunity, Luxembourg Institute of Health, 4354 Esch-sur-Alzette, Luxembourg

[11] Department of electrical engineering and computer science, University of California, CA 94720 Berkeley, USA

[12] Center for computational biology, University of California, CA 94720 Berkeley, USA

[13] Chan Zuckerberg Biohub Investigator, CA 94158 San Francisco, USA

[14] Ragon Institute of Massachusetts General Hospital, MIT and Harvard University, MA 02139 Cambridge, USA

[15] Department of Systems Immunology, Weizmann Institute of Science, 7610001 Rehovot, Israel

[16] Institute of Clinical Microbiology and Hygiene, University Hospital Regensburg and University of Regensburg, 93053 Regensburg, Germany

[17] Department of Laboratory Medicine, Medical University of Vienna, 1090 Vienna, Austria
[18] Department of Orthodontics, University Hospital Regensburg, 93053 Regensburg, Germany
[19] Department of Neurology, University of Regensburg, 93053 Regensburg, Germany
[20] Odense Research Center for Anaphylaxis (ORCA), Department of Dermatology and Allergy Center, Odense University Hospital, University of Southern Denmark, 5230 Odense, Denmark
[21] Departments of Neurology and Immunobiology, Yale School of Medicine, CT 06511 New Haven, USA
[22] Broad Institute of MIT and Harvard, MA 02142 Cambridge, USA
[23] Department of Nephrology, Medical Faculty, University Hospital Düsseldorf, Heinrich-Heine University Düsseldorf, 40225 Düsseldorf, Germany
[24] Institute for Medical Microbiology, Immunology, and Hygiene, University Hospital Cologne and Faculty of Medicine, University of Cologne, 50935 Cologne, Germany
[25] Max-Delbrück-Center for Molecular Medicine in the Helmholtz Association, 13125 Berlin, Germany

Author List Footnotes: [†]These authors contributed equally to this work. [#]These authors jointly supervised this work.

***Correspondence/Lead Contact:**

Markus Kleinewietfeld, PhD

Laboratory of Translational Immunomodulation

VIB Center for Inflammation Research (IRC)

Hasselt University, Campus Diepenbeek

Agoralaan, Building C/BIOMED, BE 3590 Diepenbeek, Belgium

Phone: +32 (0)11 26 9275

Email: markus.kleinewietfeld@uhasselt.vib.be

SUMMARY

FOXP3^{+} regulatory T cells (Tregs) are central for peripheral tolerance and their deregulation is associated with autoimmunity. Dysfunctional autoimmune Tregs display pro-inflammatory features and altered mitochondrial metabolism but contributing factors remain elusive. High salt (HS) has been identified to alter immune-function and to promote autoimmunity. By investigating longitudinal transcriptional changes of human Tregs, we identified that HS induces metabolic reprogramming, recapitulating features of autoimmune Tregs. Mechanistically, extracellular HS raises intracellular Na^{+}, perturbing mitochondrial respiration by interfering with the electron transport chain (ETC). Metabolic disturbance by temporary HS-encounter or complex III blockade rapidly induces a pro-inflammatory signature and FOXP3 downregulation, leading to long-term dysfunction *in vitro* and *in vivo*. The HS-induced effect could be reversed by inhibition of mitochondrial Na^{+}/Ca^{2+} exchanger (NCLX). Our results indicate that salt could contribute to metabolic reprogramming and that short-term HS-encounter perturb metabolic fitness and long-term function of human Tregs with important implications for autoimmunity.

INTRODUCTION

Regulatory FOXP3+ T cells (Tregs) play an essential role for the maintenance of peripheral tolerance and immune cell homeostasis[1,2]. Depending on environment and tissue, they have the ability to suppress and neutralize responses of the innate and adaptive immune system by various mechanisms like secretion of anti-inflammatory cytokines as interleukin (IL)-10 or by cell-cell contact dependent mechanism involving co-stimulatory receptors like cytotoxic T-lymphocyte-associated protein 4 (CTLA-4). Mutations in the *FOXP3* gene lead to fatal autoimmunity and dysfunctional Tregs have been linked to autoimmune disorders such as multiple sclerosis (MS), systemic lupus erythematosus (SLE), rheumatoid arthritis (RA) or type-1 diabetes (T1D) and chronic infections[1-3]. Interestingly, Treg dysfunction is frequently associated with the development of a pro-inflammatory, cytokine producing phenotype, termed Treg plasticity or fragility[4-6]. In contrast to so-called ”ex-Tregs“ that lose their Foxp3 expression in line with epigenetic alterations, fragility in Tregs is associated with the acquisition of a pro-inflammatory Th-like phenotype and loss of function, while, at least to a certain extent, maintaining *Foxp3* demethylation and expression[4,5,7-10].

High salt (HS; NaCl) content in food, associated with the so-called 'western-diet', has been established to have detrimental effects on several pathologies and autoimmune disorders by shifting the immune cell balance toward a pro-inflammatory state[11,12]. Besides impacting T effector cells (Teff), like T helper (Th)17 responses[13,14], we and others have shown that HS could also affect the function of Tregs[15-19]. HS has been shown to dynamically induce a pro-inflammatory Th1-like Treg phenotype with high expression levels of interferon (IFN)-γ and lower levels of IL-10[15,16]. Interestingly, the HS-induced Treg phenotype closely resembles dysfunctional Tregs frequently noted in patients with autoimmunity like MS[1,8]. These findings indicate that excess salt intake could contribute to an overall immune imbalance and therefore potentially represents an environmental (risk) factor contributing to disease. Despite the above findings, the exact mode of action on how salt impairs Treg function is still unknown.

Immunometabolism has gained increased attention over recent years and it is now clear that many immune reactions are governed through changes in cellular metabolism[20,21]. T cell subsets highly depend on various metabolic needs depending on environment and activation status[20]. Tregs are believed to closely mimic memory T cells in their metabolic needs, preferentially depending on oxidative phosphorylation (OXPHOS) and fatty acid β-oxidation, while Teff instead use aerobic glycolysis[20,22-26]. Several studies have highlighted the importance of mitochondrial metabolism for optimal Treg stability and function[20,24] and a recent report has demonstrated the importance of mitochondrial respiration for Treg function[27]. The ablation of mitochondrial ETC complex III in murine Tregs, by knocking-out *Uqcrfs1*, encoding for Rieske iron-sulfur polypeptide 1 (RISP), resulted in Treg loss of function and development of lethal inflammation. Interestingly, recent studies observed that Tregs isolated from patients with MS showed dampening in OXPHOS, with diminished maximal respiration levels compared to healthy controls[28,29] further displaying a deregulation of mitochondrial genes[30], indicating defects in mitochondrial function. However, factors contributing to this phenotype are unknown and if and how metabolic alterations impact the pro-inflammatory signature and function of autoimmune Tregs is poorly understood.

Very recently, two studies described the role of Na^+ in the regulation of mitochondrial function in endothelial cells, fibroblasts, monocytes and macrophages[31,32]. In endothelial cells and fibroblasts under hypoxic conditions, Na^+ acts as a second messenger that controls OXPHOS function and redox signaling. Mechanistically, Na^+ effects were mediated through the mitochondrial Na^+/Ca^{2+}

exchanger (NCLX)[31]. In monocytes and macrophages, Na^+ entered in the intracellular compartment followed by inhibition of the ETC and blunted ATP production[32]. In the present study we thus investigated the effects of HS on immunometabolism and its functional consequences for human Tregs in relation to autoimmunity.

RESULTS

HS-induced signature resembles dysfunctional autoimmune Tregs

Perturbed function of Tregs is associated with autoimmunity, however, factors contributing to this phenotype still remain elusive. Raising the extracellular salt concentration by adding extra +40mM NaCl to co-cultures of human Tregs and CFSE (Carboxyfluorescein succinimidyl ester) labeled Teffs, mimicking physiologically increased Na^+ concentrations found in interstitial tissues after HS diets[11,33,34] or during inflammation[35], significantly inhibited the suppressive capacity of human Tregs *in vitro* (**Figures 1A and S1A**). The effect could already be observed at lower NaCl concentrations starting from +10mM NaCl, and it was neither due to changes in osmotic pressure, since addition of mannitol as a tonicity control did not affect suppressive function of Tregs, nor by acting directly on Teffs (data not shown)[15]. Furthermore, the HS effect on Tregs could also be observed in more physiological *in vitro* assays. Salt-treated Tregs were unable to efficiently suppress allogeneic activation in mixed lymphocyte reactions (MLR; **Figure S1B**)[36] and displayed diminished suppressive capacity on Teffs in the presence of dendritic cells (DCs; **Figure S1C**)[37]. In line with previous reports[15,16], high-sodium conditions induced IFN-γ expression in Tregs (**Figure S1D**) and a higher proliferation of Tregs in suppression assays (**Figure 1B**), characteristic for dysfunctional Tregs observed in autoimmunity and indicative of Treg metabolic reprogramming under HS exposure.

In order to better understand salt-induced molecular changes and to investigate a potential overlap between HS-treated Tregs and dysfunctional autoimmune Tregs, we performed bulk-RNA sequencing (RNA-seq) of Tregs that were cultured under HS and control conditions for a period of 72 h and compared the expression signature to published RNA-seq datasets of Tregs isolated from patients with different autoimmune diseases (**Figure 1C).**[30] Gene set enrichment analysis (GSEA) revealed “Hallmarks of Interferon gamma response” as one of the top upregulated pathways after HS exposure with 69 enriched genes (NES = 1.63; false discovery rate [FDR] =

0.007; **Figure 1C**). In line with this, the expression pattern of Tregs isolated from five healthy individuals was strongly indicative of a pro-inflammatory Th1-like phenotype, with the upregulation of key Th1-associated genes like *CXCR3, TBX21*/*T-bet*, and *IFNG* and other signature genes and activation markers upon HS exposure (**Figure S1E**).

Importantly, GSEA analysis and investigation of Th1-like signatures of Tregs from patients with MS, SLE and RA[30] showed a similar strong and top enrichment of "Hallmarks of Interferon gamma response" with 70 genes being enriched in the MS cohort (NES = 1.44; FDR = 0.031), 129 genes in the SLE cohort (NES = 2.62; FDR = 0.000) and 108 genes in the RA cohort (NES = 1.54; FDR = 0.022), indicating highly overlapping and common functional features between the autoimmune and HS datasets (**Figure 1C** and data not shown). This observation goes well in line with our results on a higher IFN-γ expression after HS treatment (**Figure S1D**), as well as with previously studies on the acquisition of a Th1-like phenotype in Tregs of patients with MS[16] and Tregs exposed to HS environments[15]. Thus, our data show that HS induces a dysfunctional Th1-like phenotype in Tregs that closely mimics key gene expression signatures and functional features of Tregs isolated from patients with autoimmunity.

Salt-induced Treg dysfunction is associated with severe changes in immunometabolism

Since we observed highly overlapping signatures between 72-h HS-exposed Tregs and Tregs isolated from patients with autoimmunity[30] and both showed indications for immunometabolic remodeling, we hypothesized that salt effects cellular immunometabolism of Tregs, particularly at early stages. Thus, in order to investigate the functional consequences of HS on Tregs in more detail, we analyzed changes in gene expression under HS exposure over time. Human Tregs were activated *in vitro* for 6 h and compared to those activated for 72 h in the presence or absence of HS, and gene expression was analyzed by bulk RNA-seq in comparison to *ex vivo* isolated Tregs without prior activation (**Figure 2A**). Of note, the impact of HS on gene expression was much more pronounced at 6 h post activation as compared to 72 h, indicating that HS induces particularly profound changes in gene expression of Tregs at early stages of activation (**Figure 2A**). When analyzing the 6-h time point in detail, we identified 1,250 upregulated and 1,380 downregulated genes (FDR < 0.05) under HS exposure (**Figure 2A**). Among the highest regulated genes under HS were candidates belonging to the catenin pathway (*CTNN1*, *DACT3*,

and TCF7), previously shown to be critically affected by HS[16] as well as key effector molecules for Tregs such as *IL10* (**Figure 2B**). Meanwhile, further in agreement with previous reports, the expression of *IFNG* was not majorly affected at 6 h and only developed in line with the HS-induced dynamic induction of a Th1-like Treg signature at later time points, resulting in an increased *IFNG*/*IL10* ratio (**Figures S1F and S1G)**[15,16]. Interestingly, the early expression analysis of HS-treated Tregs also indicated severe changes in cellular metabolism. Further, among the highest regulated genes we found genes associated with mitochondrial function (*OMA1, ETFB*, and *BCAT2;* **Figure 2B**). To investigate the consequences of HS at 6 hours post activation in more detail, we applied single-cell RNA-seq (scRNA-seq) on Tregs (**Figure S2A)** treated under HS or control conditions. The tSNE projections were performed on 4,785 cells and 10 clusters were identified (**Figure 2C**). HS-treated Tregs were highly differentially represented within the clusters. While in clusters 0 and 3 there was an overrepresentation of HS-treated Tregs; clusters 1, 2, and 4 depicted an underrepresentation of these cells (**Figures 2C and S2B**).

In order to explore the metabolic features of HS-treated Tregs, we used the Compass algorithm[38], which utilizes flux-balance analysis to infer metabolic states of cells based on scRNA-seq. Compass analysis indicated shifts in several metabolic pathways, pointing toward a severely altered metabolic state of HS-exposed human Tregs (**Figure 2D**). Importantly, the analysis revealed downregulation of key nodes for pyruvate metabolism and tricarboxylic acid (TCA) cycle after HS exposure, whereas the urea cycle was detected as being upregulated (**Figure 2D**). Within the TCA cycle, several reactions and enzymes were found to be affected, such as succinate dehydrogenase (SDH), malate dehydrogenase, and isocitrate dehydrogenase (**Figure 2E**). SDH drives the enzymatic conversion of succinate to fumarate, playing a pivotal role in OXPHOS as the electron acceptor complex II. Inhibition of this enzyme leads to the accumulation of succinate, diminishing electron passage through the ETC, resulting in a downregulation of OXPHOS capacity[39]. Furthermore, accumulation of succinate and downregulation of *SDH* was shown to impair T cell activation and production of anti-inflammatory cytokines[39].

In order to investigate potential changes on the metabolite levels, we applied liquid chromatography-mass spectrometry (LC-MS) of Tregs that had been cultured under control or HS conditions (**Figure S2C)**. Our data revealed an upregulation of succinate under HS conditions, corroborating with the detected downregulation of *SDH* through Compass analysis (**Figure 2E)**.

Moreover, an accumulation of fumarate was observed, which can potentially be linked to the observed upregulation of the urea cycle (**Figure 2D)**. Furthermore, we also detected an upregulation of malate alongside a downregulation of NADH and NADPH (**Figure S2C)**. These results go well in line with the Compass predictions, where a downregulation of malate dehydrogenase inhibits the conversion of malate to oxaloacetate resulting in higher levels of malate and a diminished production of NADH. In line with the above findings, GSEA analysis on the scRNA-seq data showed “Hallmark of oxidative phosphorylation” as the most downregulated pathway, with 149 genes affected (NES = 2.4; FDR = 0.001), after HS-exposure for 6 h (**Figure 2F**). This was further independently corroborated by IPA analysis, identifying OXPHOS as being the top downregulated pathway after HS exposure (data not shown). In summary, our data demonstrate that salt exposure induces massive shifts in gene expression particularly at early time points, indicative for a severe deregulation in Treg immunometabolism.

High salt inhibits oxidative phosphorylation of Tregs

Since the RNA-seq and scRNA-seq data pointed toward a disturbed mitochondrial metabolism of HS-treated Tregs, we investigated their respiratory capacity by assessing oxygen consumption rate (OCR). Seahorse profile at 72 and 24 h post activation revealed that Treg maximal respiration was significantly reduced after salt-exposure (**Figures 3A, 3B,S2D and S2E**), which was not due to alterations in cell viability (**Figure S2F**). To independently confirm the data, we analyzed ATP production of human Tregs directly. In line with the previous results, HS Tregs showed a dramatic reduction of ATP production, even to a similar extent as compared to oligomycin exposure, a potent inhibitor of mitochondrial complex V of the ETC at 6 h post activation (**Figure 3C**). To examine whether changes in mitochondrial mass could account for the observed effects, we analyzed mitochondria of Tregs by FACS using Mitotracker. No changes were observed between HS and control conditions, indicating that the effects were not due to changes in mitochondrial mass (**Figure S2G**). In line with these findings, analysis of HS and control activated human Tregs by transmission electron microscopy (tEM) did not reveal any major morphological changes (**Figures 3D and S2H**).

We next tested if HS led to changes in mitochondrial membrane potential (Ψm) by tetramethylrhodamine ethyl ester (TMRE) staining. As controls we used carbonyl cyanide p-

(trifluoromethoxy)phenylhydrazone (FCCP), a potent uncoupler of Ψm and antimycin A (AA), a specific inhibitor of complex III. Of note, HS led to a collapse of the mitochondrial membrane potential and significantly reduced TMRE signal even to a comparable extent to AA at 6 h post activation **(Figure 3E**). Furthermore, we observed increases in mitochondrial reactive oxygen species (mtROS) after HS exposure in human Tregs (**Figure S2I**). Based on the above results, we thus hypothesized that salt may interfere with cellular metabolism by disturbance of mitochondrial respiration at the level of the ETC.

To investigate the effect of HS on mitochondrial respiration in more detail, we analyzed the transcriptional profile of activated human Tregs after 6 h under inhibition of complex III by AA. Interestingly, RNA-seq analysis revealed a highly overlapping gene expression signature of top significant genes upon HS and AA treatment (FDR < 0.05; **Figure 3F**), indicating the activation of a similar expression program. Previous data showed that the deletion of RISP induced a distinct gene expression pattern that was mimicked closest by treatment of murine Tregs by AA[27]. Strikingly, by comparing our RNA-seq data from human Tregs (HS vs. CTRL and AA vs. CTRL) with the published murine expression data on AA treatment and chimeric RISP knockout (KO ; AA vs. CTRL in murine Tregs and RISP KO vs. wildtype [WT] murine Tregs)[27], we found highly overlapping gene signatures with the OXPHOS pathway being the top hit (z score ≤ -6; **Figure 3G**). In summary, our results demonstrate that HS severely disturbs Treg mitochondrial respiration. The similarities of datasets between HS treatment and interfering with ETC complex III indicate that sodium affects Treg mitochondrial metabolism on a similar level.

Perturbation of mitochondrial metabolism severely alters the function of human Tregs

To dissect the mechanistic consequences of HS-perturbed mitochondrial function of Tregs, we analyzed the expression data for functional changes on Tregs treated under HS or AA. Intriguingly, the scRNA-seq data at 6 h post activation identified the transcription factor *FOXP3* as one of the most downregulated genes after HS exposure (**Figure 4A**). Downregulation of *FOXP3* expression after HS exposure for 6 h was independently confirmed by real-time qPCR (**Figure 4B**) and by FACS at the protein level, measured after 24 h of activation under similar conditions (**Figure 4C**). In line with this, the incubation of T cells with AA also led to a significant reduction of FOXP3 expression (**Figure S3A**). Since FOXP3 is essential for Treg stability and

function[1-3,14], its intriguing to speculate that the rapid downregulation of FOXP3 expression after HS exposure could account for the observed loss of function in Tregs. In the light of these findings, it is of interest that recent data revealed a direct link between FOXP3 expression and OXPHOS[40]. In line with the downregulation of FOXP3, the expression pattern of other essential Treg genes resembles that of non-functional Tregs (**Figure 4D**) [8]. Downregulation of *IL10* and *CTLA4* as well as the upregulation of *SATB1* indicated a strong pro-inflammatory bias of HS or AA on Tregs and were independently confirmed by qRT-PCR and protein expression analysis for CTLA4 and IL-10 by FACS (**Figures 4E,4F, S3B and S3C**). Further, STAT5 phosphorylation, indicative for IL-2 responsiveness, was significantly hampered under HS and AA conditions (**Figures 4G and S3D**). To investigate if the inhibition of complex III abrogates suppressive function of human Tregs as compared to HS treatment (**Figure 1A**), we analyzed the effects of AA in *in vitro* suppression assays. To exclude any direct impact on Teffs, Tregs were pre-activated for 72 h in the presence of AA or HS and subsequently tested for their suppressive function under standard conditions (**Figure 4H)**. Importantly, similar to HS pre-activation, the inhibition of complex III by AA significantly abrogated Treg function, indicating that the interference by either pharmacological inhibition or salt-mediated perturbation of mitochondrial function leads to equal functional consequences *in vitro* (**Figure 4H**). To further confirm these results, we applied CRISPR-Cas-mediated KO of the RISP gene in human Tregs(**Figure S3E**)[41]. To analyze if the ablation of *UQCRFS1* in Tregs induces a similar phenotype as the pharmacological inhibition of complex III or HS exposure, RISP-KO Tregs were tested in *in vitro* suppression assays. As expected, based on our IPA comparison analysis (**Figure 3G**) and previous findings in mice[27] the deletion of the RISP gene in human cells resulted in lack of suppression *in vitro*, closely resembling the dysfunctional phenotype of HS- and AA-treated Tregs (**Figure 4I**). In line with the above results, RISP-KO Tregs further displayed an increased *IFNG/IL10* ratio (**Figure S3F**).

Salt-induced inhibition of mitochondrial function disrupts Treg fitness and function *in vivo*

To investigate if high sodium intake may affect the phenotype of human Tregs *in vivo*, we analyzed Tregs in respect to individual salt intake of healthy volunteers (**Figures 5A-C**). Daily salt consumption of participants was calculated based on a dietary questionnaire covering individual food habits as described before,[42] and volunteers were grouped into “low salt” (LS) and HS based

on a cutoff of 7g/day NaCl intake (**Figure 5A**). Strikingly, the analysis of Tregs revealed a significant reduction of IL-10 expression in Tregs from the HS group in comparison to the LS group (**Figures 5B and S4A**), and the percentage of IL-10 expression in Tregs negatively correlated with salt intake in a significant manner (**Figure 5C**). However, we only observed tendencies for decreases in FOXP3 and increases in IFN-γ expression in the HS group (data not shown).

Previous reports have shown that HS inhibits the function of murine thymic-derived Tregs[15,19] and murine *in vitro* suppression assays under HS conditions independently confirmed these findings (**Figure S4B**). In order to directly dissect the impact of HS on murine Treg fitness and function, we performed an adoptive transfer experiment of murine Tregs to contain experimental autoimmune encephalomyelitis (EAE). In this model the adoptive transfer of Tregs was shown to significantly ameliorate EAE, presumably in dependence of Treg-derived IL-10 production[43,44]. EAE was induced and Tregs were isolated from naïve donor mice and pre-incubated in either control or HS conditions and injected into recipient mice after 6 days of EAE induction (**Figure 5D**). Of note, animals receiving salt pre-treated Tregs failed to contain the development of EAE, resulting in significantly higher disease scores (**Figure 5E**).

To investigate if the short-term disturbance of mitochondrial function of human Tregs by HS or AA would similarly have long-term consequences *in vivo*, we used the model of xenogeneic graft vs. host disease (xGvHD) in immunodeficient mice[15,36,45]. We pre-incubated human Tregs (**Figures S4C and S4D)** under HS, AA, or control conditions for 6 h before co-injection with CD25-depleted PBMCs into NOD.Cg-Prkdc^{scid}Il2rg^{tm1Wjl}/SzJ (NSG) mice to monitor their *in vivo* potential to contain xGvHD compared to controls (**Figure 5F**). Injected effector cells and Tregs of all four groups engrafted equally well as verified by FACS (**Figures S5A and S5B**). Weights of the mice together with survival rates were monitored, and weight loss in controls occurred around day 25 (**Figure S5C**). Importantly, only mice receiving CD25-depleted PBMC together with untreated control Tregs were significantly able to prevent severe xGvHD. HS or AA pre-treated Tregs were unable to restrain disease in CD25$^-$ PBMC receiving animals (**Figure 5G**). Further, analysis of splenocytes showed that only animals receiving functional Tregs displayed a lower percentage of human CD8$^+$ T cells, known as major drivers of xGvHD (data not shown) [46,47]. In summary, our

data demonstrate that even the short-term HS perturbation of mitochondrial respiration could lead to long-term disruption of human and murine Treg function *in vivo*.

Salt-induced mitochondrial dysfunction depends on mitochondrial NCLX

Recent reports have shown that extracellular HS conditions lead to subtle increases of intracellular Na^+ in macrophages[48,49]. To examine if this phenomenon is also observed in adaptive immune cells, we tested if the incubation under HS conditions leads to increases of the intercellular Na^+ content in $CD4^+$ T cells (**Figure 6A**). Indeed, extracellular HS conditions raised intracellular Na^+ levels to a similar range as observed in macrophages[32,48,49], and this effect was already observed at lower HS conditions (+10mM NaCl), although to a lesser extent (**Figure S6A**). In order to directly examine the impact of HS conditions on the ETC, we analyzed effects of increased Na^+ on the activity of complex II and complex III (**Figures 6B and 6C**). We tested complex II activity in the presence of +4mM NaCl, reportedly in the physiological range of the cytosol under HS-conditions[48,49]. Complex II function was diminished by almost 50% in a cell- and mitochondrion-free assay, indicating that increased intracellular Na^+ could directly affect late complex II activity of human Tregs (**Figure 6B**). We next investigated the combined complex II/III function in intact purified mitochondria upon increased NaCl concentrations. NaCl dose-dependently inhibited complex II/III activity to a similar extent as AA (**Figure 6C**). Thus, our data indicate that HS induces a disturbance of mitochondrial respiration in Tregs at the level of complex II/III of the ETC.

A recent study has demonstrated that Na^+ influx into mitochondria under hypoxic conditions is regulated by the mitochondrial Na^+/Ca^{2+} exchanger NCLX, interfering with OXPHOS function[31], mirroring our previously observed effects of Tregs under HS. Considering HS-induced increases in intracellular Na^+ and direct effects on complex II/III activity, we tested the effects of a specific inhibitor of NCLX (CGP-37157; CGP) on complex II/III activity. CGP significantly reversed salt-induced decrease of complex II/III activity, indicating that mitochondrial influx of Na^+ mediates the HS-induced effect on the ETC **(Figure 6D**). To examine, if this effect is also directly observed in Tregs, we analyzed the impact of NCLX inhibition under HS conditions in suppression assays. Human Tregs were pre-activated under HS-conditions in the presence or absence of CGP and were tested for their function. Notably, pharmacological inhibition of NCLX in Tregs under HS

environments, led to a significant recovery of suppression (**Figure 6E**). Furthermore, in line with increases of *FOXP3*, Treg incubation with CGP was able to significantly reduce the *IFNG/IL10 ratio* (**Figures 6F and S6B**), indicating that CGP inhibits the Th1-like pro-inflammatory phenotype conferred by HS treatment. CGP further partially restored HS-perturbed Treg function *in vivo*. The inhibition of NCLX in Tregs led to increased potency to contain EAE and xGvHD (**Figures S6C and S6D**). Thus, mechanistically, mitochondrial Na^+ influx induced by extracellular HS conditions and its direct effects on the ETC in Tregs through NCLX seem to be key for the observed immunometabolic disturbance and dysfunction of HS-treated human Tregs, closely mirroring autoimmune Tregs (**Figure 6G**).

Discussion

Here we have demonstrated for the first time that HS severely affects cellular metabolism and suppressive function of Tregs. We observed that HS leads to a pro-inflammatory Th1-like profile, which closely overlaps with the transcriptomic features of Tregs isolated from patients with autoimmune disorders. Our data demonstrate that raised physiological HS conditions, similar to Na^+ concentrations that can be reached inside inflamed tissues *in vivo*, perturb the function of Tregs by metabolic reprogramming through the interference with mitochondrial respiration.

Mechanistically, Na^+ is taken up to the intracellular compartment and subsequently via NCLX to the mitochondria, where it directly blocks mitochondrial respiration on the level of complex II/III of the ETC, leading to significantly decreased OCR and mitochondrial membrane potential and consequently to lower ATP levels. This energy obstruction based on HS-induced mitochondrial dysfunction seems to be the initial step for how sodium alters Treg function and leads to a swift downregulation of FOXP3 and massive changes in gene expression, in line with significant phenotypic and functional alterations, closely mimicking dysfunctional Tregs in autoimmunity[8,15,16]. A similar phenotype can be induced by pharmacological blockade or interference with complex III by AA, and our data demonstrate that the HS-induced effect on Treg dysfunction could be reversed by inhibition of mitochondrial Na^+ influx through blocking of NCLX. Importantly, our data provide evidence that even the short-term disruption of mitochondrial function can have long-lasting consequences for the fitness and suppressive capacity of human and murine Tregs. Similar processes may occur in humans *in vivo*, linking dietary salt intake to

immune function and defining it as a potential risk factor contributing to disease. By now, already a few studies reported that even moderate changes in salt intake could impact human immunophenotypes[11]. Our data, although only on a limited number of individuals, show a significant negative correlation of IL-10 expression in FOXP3$^+$ Tregs in relation to higher salt intake in healthy subjects. However, these findings need to be validated in larger follow-up studies.

Our data go well in line with recent studies that indicated that Tregs of people with MS display a disturbed metabolic phenotype and defects in mitochondrial respiration[28,29] and that autoimmune Tregs show a signature of mitochondrial dysfunction[30]. It is thus tempting to speculate that perturbed mitochondrial function elicited by HS encounter, copying hallmarks of dysfunctional Tregs in autoimmunity, further provides a piece of evidence linking environmental factors and shifts in the ionic microenvironment to the observed deregulation of the immune cell balance[3].

Tregs not only play a role in autoimmunity but have also been shown to be important mediators to contain chronic inflammation in cardiovascular diseases (CVDs) such as atherosclerosis[50], hypertensive target organ damage[51] and myocardial infarction[52]. Interestingly, reduced Treg numbers and a dysfunctional Treg phenotype have also been reported in CVD and were associated with progression of disease[53-56]. Since Tregs in CVD also displayed a pro-inflammatory Th1-like phenotype[57,58], it would be of interest to investigate if excess sodium may further contribute to chronic inflammation and CVD by disabling Tregs.

In this respect, it is notable that HS-perturbed Tregs seem to rather resemble “fragile” Tregs than “ex-Tregs”. While exhibiting decreases in FOXP3, HS-perturbed Tregs still largely maintained demethylation of the *FOXP3* locus and showed a Th-like phenotype and further expression of characteristic markers for Treg fragility (data not shown). Although this becomes a detrimental scenario in autoimmunity or CVD, it can be beneficial in cancer, promoting more efficient anti-tumor immunity[4,5,7], indicating that the mechanistic insights on how HS acts on Tregs may of further interest in the field of cancer.

It is tempting to speculate that the discovery of the metabolic effect of salt on Tregs also applies for other salt-sensitive immune cell types like Th17 cells[13,14] or myeloid cells[59,60] and therefore may have a general impact on regulating immune reactions in response to changes in the ionic microenvironment. Earlier studies in the murine system have already indicated that HS affects

cellular metabolism of macrophages[61,62]. Further, Hernansanz-Augustin and colleagues demonstrated that hypoxia activates NCLX, resulting in an accumulation of cytosolic Ca^{2+} and subsequent Na^{+} accumulation in mitochondria[31], which resulted in lower membrane fluidity and diminished complex II/III activity, ultimately leading to a burst of superoxide and reduced ATP production. These findings go well in line with our data in human Tregs, where increases in Na^{+} seem to directly interfere with late complex II and complex III activity, leading to the described phenotypic and functional consequences for human Tregs even in the absence of hypoxic conditions, suggesting a common cell type-independent mechanism for how Na^{+} could affect OXPHOS. Since the inhibition of NCLX reversed the salt-induced Treg dysfunction, our findings indicate that this mechanism may represent a potential target to restore Treg function under conditions of altered ionic microenvironments or hypoxia. However, since CGP as an inhibitor of NCLX[63] showed limited specificity by also effecting the plasma membrane Na^{+}/Ca^{2+} antiporter SLC8A1[64,65], further research is needed to overcome these issues in the future. Although CGP was successfully used to prevent heart failure and sudden cardiac death[66], tamoxifen-induced cardiomyocyte-specific deletion of *Slc8b1* in adult mouse hearts resulted in fatal outcomes[67]. These reports indicate on the complexity of potentially targeting NCLX *in vivo*. However, several attempts have already been made to optimize CGP specificity and pharmacokinetic profile by the generation of new analogs, which might be superior for potential future therapeutic usage[68,69]. Moreover, novel targeted approaches and strategies may further allow cell type and mitochondria-specific applications in the future[70].

In summary, we have demonstrated for the first time that HS perturbs mitochondrial function of human Tregs by inhibition of mitochondrial respiration on the level of ETC complex II/III. The critical disturbance of energy production induces metabolic reprogramming in Tregs and goes in line with severe changes in gene expression and functional alterations. The HS effect could be mimicked by pharmacological inhibition or genetic disruption of mitochondrial complex III, leading to a similar phenotype observed in dysfunctional Tregs of patients with autoimmunity, and our data indicate that salt-intake could impact functional features of human Tregs. Since even the short-term engagement in HS environments could lead to long-term loss of function of Tregs, our findings may have important implications for autoimmunity. The interference with this pathway by

targeting mitochondrial NCLX may offer novel treatment options for salt-sensitive diseases but warrants further investigation.

Limitations of Study

We acknowledge some limitations within our study. Since the majority of experiments were conducted with human specimen, we appreciate it's intraindividual variability and genome editing in human Tregs did not reach complete KO. Due to a limited number of participants in the salt-intake study, our findings should be further followed up in larger, randomized placebo-controlled studies. Moreover, we cannot fully exclude putative off-target effects of the NCLX inhibitor used. Since the exact physiological mechanism of how sodium distributes inside tissues and exerts its function on immune cells is still not well understood[11,71,72], it would be interesting to investigate this in more detail with respect to Treg function.

ACKNOWLEGMENTS

We thank Anneleen Geuzens, Dries Swinnen, Stefaan Dervaux, Niels Vandamme, Bart Ghesquière, Camila Takeno Cologna, Riet de Rycke, Saskia Lippens, Thomas Bartolomaeus and Anja Maehler for technical assistance and support. S.G. was supported by the Bundesministerium für Bildung und Forschung (BMBF) funding MSTARS. J.J. received funding from the DFG (German Research Foundation) (JA1993/6-1) and SFB 1350 grant (387509280, TPB5). D.N.M., H.B. were supported by the DFG (394046635– SFB 1365); D.N.M. was also supported by the DFG (SFB-1470 - A06) and by the Deutsches Zentrum für Herz-Kreislauf-Forschung (DZHK, 81Z0100106). D.B. and H.K. were supported by the FNR-ATTRACT program (A14/BM/7632103) and D.B. by FNR-CORE grant (C18/BM/12691266) of the Luxembourg National Research Fund. Y.S. and J.R. were supported by the Flemish Government under the "Onderzoeksprogramma Artificiële Intelligentie (AI) Vlaanderen" program. D.A.H received funding from the National Institutes of Health (NIH) (U19 AI089992, R25 NS079193, P01 AI073748, U24 AI11867, R01 AI22220, UM 1HG009390, P01 AI039671, P50 CA121974, and R01 CA227473), the National Multiple Sclerosis Society (NMSS) (CA1061-A-18 and RG-1802-30153). M.K. was supported by the European Research Council (ERC) under the European Union's Horizon 2020 research and innovation program (640116) and by a SALK-grant from the government of Flanders and by an

Odysseus-grant (G0G1216FWO) and senior research project (G080121N) of the Research Foundation Flanders, Belgium (FWO) and by a BOF grant (ADMIRE, 21GP17BOF) from Hasselt University.

AUTHOR CONTRIBUTIONS

B.F.C.R. and I.H. designed and performed most experiments, analyzed and interpreted the data. R.A.H, L.V.Z., S.G., A.D., H.K., S.N.Y.W., K.G.S., A.S., J.J., S.H., L.K. and H.B. performed experiments and analyzed data. J.R. and Y.S. performed analysis on tEM micrographs and interpreted data. M.V.G and L.D. assisted with Seahorse experiments and interpreted data. A.W., N.Y., N.H., R.L., D.B., J.S., S.K. and D.A.H. gave conceptual input. D.N.M. supervised experiments and interpreted data. M.K. led and conceived the project, supervised experiments, interpreted data. B.F.C.R, I.H. and M.K. wrote the manuscript with key editing by S.G. and D.N.M. and further input from all authors.

DECLARATION OF INTEREST

The authors declare no competing interests.

INCLUSION AND DIVERSITY

We support inclusive, diverse, and equitable conduct of research.

FIGURE LEGENDS

Figure 1. **Salt-induced changes in Treg phenotype and function closely mimic human autoimmune Tregs. (A)** $CD4^+$ Teffs were labeled with CFSE and co-cultured with Tregs (1:1 ratio) under control (CTRL) or HS media (+40mM NaCl). Teff proliferation was measured after 4 to 5 days of incubation. Representative Teff proliferation shown in histograms (left) and percentage of proliferation of HS group (red) were calculated by normalizing to CTRL group (black) (right, n = 12 from six independent experiments). **(B)** Treg proliferation was assessed by CTV-dilution after 4 to 5 days of incubation in suppression assays under CTRL or +40mM NaCl conditions. Representative FACS-plots (left) and quantification of proliferation (right) are shown (n = 12 from five independent experiments). **(C)** Enrichment plots (GSEA) of IFN-γ response of

bulk RNA-seq from Tregs activated under HS (+40mM NaCl n = 5) or control conditions (CTRL n = 5) for 72 h (top left) and of isolated Tregs from peripheral blood of healthy individuals (n = 14) and subjects with MS (n = 10, top right), SLE (n = 8, bottom left), and RA (n = 9, bottom right). The RNA-seq data from healthy individual- and patient-derived Tregs were downloaded from the European Genome-phenome Archive (EGA: EGAS00001004470[30]) and reanalyzed accordingly. For **(A and B)** data are depicted as mean ± SEM. **p < 0.01, ***p < 0.001. Normal distribution was calculated by Shapiro-Wilk normality test with a significance level of 0.05. Significance was calculated by paired two-tailed t test for normal distributed data.

Figure 2. High salt (HS) induces discrete changes in gene expression in human Tregs indicative for metabolic reprogramming. (A) Heatmap showing changes in gene expression of unstimulated Tregs (0 h) and Tregs after 6- and 72-h activation under CTRL or +40mM NaCl conditions. Each column contains the average measurements for differential gene expression by RNA-seq for two to five biological replicates. **(B)** Volcano plot of differentially expressed genes (DEGs) in HS vs. control activated Tregs for 6 h. **(C-F)** scRNA-seq analysis of Tregs incubated under CTRL conditions or +40mM NaCl for 6 h. **(C)** T-distributed stochastic neighbor embedding (tSNE) plot showing clustering of 4,785 cells based on gene expression divided into 10 different clusters. Individual points correspond to single cells colored according to clusters (left) and conditions (right). **(D)** Compass-based exploration of metabolic heterogeneity within Tregs. Compass results of the modeled metabolic landscape in Tregs activated for a period of 6 h in the absence (CTRL) or presence (+40mM NaCl) of HS media. **(E)** Compass-score differential activity test of TCA cycle pathway between +40mM NaCl vs. control-treated cells. Each dot represents a single biochemical reaction. **(F)** Enrichment plot (GSEA) of OXPHOS of scRNA-seq from Tregs activated under +40mM NaCl or control conditions (CTRL) for 6 h.

Figure 3. **High salt (HS) inhibits mitochondrial respiration in human Tregs. (A-B)** OCR of Tregs activated under control (black) or +40mM NaCl conditions (red) for a period of 72 h. Overlay of OCR tracer (**A**) and maximal OCR (**B**) of control and +40mM NaCl cultured Tregs after 72 h of activation (n = 10 from seven independent experiments). **(C)** Relative ATP content of 6-h activated Tregs under control (CTRL) or +40mM NaCl conditions (n = 7 from three independent

experiments). Oligomycin treatment was used as positive control (n = 5 from two independent experiments). **(D)** Representative electron micrographs of activated Tregs in CTRL or +40mM NaCl for 6 h (scale bar, 2µm). **(E)** Relative TMRE MFI in Tregs activated for a period of 6 h under CTRL or +40mM NaCl conditions and in the presence of AA or FCCP (n = 8 from four independent experiments). **(F)** Heatmap from RNA-seq profiles of Tregs activated under CTRL or +40mM NaCl conditions or in the presence of AA for 6 h (adjusted $p < 0.05$). Each column represents a single sample, datasets for CTRL and HS conditions were adapted from Figure 2A. **(G)** Ingenuity Pathway Analysis (IPA) predictions on comparison analysis of 6-h activated human Tregs under CTRL vs. +40mM NaCl conditions and CTRL vs. AA conditions and on publicly available transcriptomic data of murine Tregs (CTRL) vs. AA treated Tregs (AA) (CTRL vs. AA, murine) and RISP chimeric WT vs. RISP chimeric KO Tregs (WT vs. RISP KO, murine)[27]. **(A-C and E)** data are depicted as mean ± SEM. *$p < 0.05$, **$p < 0.01$, ***$p < 0.001$, ****$p < 0.0001$. Normal distribution was calculated by Shapiro-Wilk normality test with a significance level of 0.05. Significance was calculated by paired two-tailed t test for normal distributed data **(B**), by Holm Sidak's multiple comparison test (**C**), or by Friedman test with Benjamini-Hochberg FDR-correction (**E**).

Figure 4. Salt-mediated disruption of mitochondrial respiration perturbs human Treg function. (A-C) FOXP3 expression after HS exposure on Tregs activated under CTRL or +40mM NaCl conditions. **(A)** Volcano plot of DEGs obtained from analysis of the scRNA-seq data of 6-h activated Tregs under control and +40mM NaCl conditions. **(B)** Relative gene expression of *FOXP3* in Tregs activated for 6 h under CTRL or +40mM NaCl conditions assessed by qRT-PCR (n = 5 from three independent experiments). **(C)** FACS analysis of FOXP3 expression in isolated Tregs, activated for 24 h under control or HS-conditions. FACS plots (left) and a dotplot (right) showing MFI levels normalized to the control group are depicted (n = 5 independent donors). **(D-G)** Cells were activated under control, HS conditions, or in the presence of AA. **(D)** Heatmap showing differential expression in a selected set of genes of activated Tregs at 6 h. Each column contains the average measurements for differential gene expression by RNA-seq for three to five biological replicates. **(E)** Relative gene expression of *IL10* and *CTLA4* in Tregs activated for 6 h under control, HS conditions, or in the presence of AA assessed by qRT-PCR (n = 7-9 from four

to five independent experiments). **(F)** FACS analysis of IL-10 and CTLA4 expression in the FOXP3$^+$ Tregs of total CD4$^+$ T cells, activated for 24 h under CTRL or +40mM NaCl. A representative FACS plot (left) alongside a dotplot (right) showing percentage normalized to the control group is depicted (n = 4 independent donors). **(G)** pSTAT5 assessed in Tregs activated for a period of 4 h under control, HS-conditions, or in the presence of AA by FACS. Dotplot depicts MFI levels alongside a representative histogram plot (n = 5-8 from two to three independent experiments). **(H)** Tregs were pre-incubated under control, HS-conditions, or in the presence of AA for 72 h and then co-cultured with CFSE labeled Teffs at a 1 to 1 ratio. Teff proliferation was assessed after 4 days (n = 6 from four independent experiments). **(I)** Human RISP KO and Mock CTRL Tregs were co-cultured with CFSE-labeled total PBMCs at a 1 to 3 ratio (n = 3 from 2 independent experiments). For **(B,C, and E-I)** data are depicted as mean ± SEM *p < 0.05, **p < 0.01, ***p < 0.001, ****p < 0.0001. Normal distribution was calculated by Shapiro-Wilk normality test with a significance level of 0.05. Significance was calculated by paired two-tailed t test for normal distributed data (**B, C, H, and I**), or one-tailed t test (**F**), by Friedman test with Benjamini-Hochberg FDR-correct (**E**), or by one-way ANOVA with Tukey's post-hoc test (**G**).

Figure 5. Impact of salt on Treg fitness and function *in vivo.* (A-C) Salt intake and its impact on Tregs in healthy human subjects. **(A)** Healthy individuals were separated into two groups based on their daily salt intake (LS = low salt, [<7g NaCl/day]; HS = high salt [>7g NaCl/day]). **(B)** Analysis of IL-10 expression in FOXP3$^+$ Tregs of PBMCs isolated from participants. A representative FACS plot (left) and quantification (right) of IL-10$^+$ cells is depicted (n = 8/HS and n = 10/LS independent donors). **(C)** The Spearman Correlation scatterplot showing the association between percentage of IL-10$^+$FOXP3$^+$ Tregs and daily salt intake (g) in healthy volunteers (n = 18). The black line corresponds to the regression line (correlation R = -0.67; p = 0.0023). **(D-E)** Impact of salt on Treg fitness and function to contain EAE by adoptive transfer. **(D)** EAE was induced in recipient mice and CD4$^+$CD25$^+$ Tregs of naïve donor mice were pre-incubated in the presence of +40mM NaCl or control conditions for 24 h prior to being adoptively transferred into recipient mice 6 days after EAE induction. **(E)** Mice were kept for a period of 15 days post induction and monitored daily for the development of EAE symptoms (n = 4-5 per group from two independent experiments). **(F-G)** Impact of salt on human Treg fitness and function to

contain xGvHD. **(F)** Schematic experimental set-up for xGvHD. Human $CD25^+$ Tregs were activated in control media, media supplemented with AA or media supplemented with +40mM NaCl for 6 h. Pre-incubated Tregs were mixed with autologous $CD25^-$ PBMCs and injected into NSG mice (PBMC alone [blue]; PBMC and Treg CTRL [black]; PBMC and Treg NaCl [red]; PBMC and Treg AA (orange) n = 5-6/group). Mice were monitored for a period of 60 days for development of xGvHD. **(G)** Survival rates of xGvHD experiment over time. **(A, B, E)** data are depicted as mean ± SEM. *p < 0.05, **p < 0.01, ****p < 0.0001. Normal distribution was calculated by Shapiro-Wilk normality test with a significance level of 0.05. Significance was calculated by unpaired two-tailed t test for normal distributed data (**A and B**), by Mann-Whitney test for separate days during EAE development (**E**), or by curve comparison analysis using Mantel-Cox and Gehan-Breslow-Wilcoxon tests (**G**).

Figure 6. Salt-induced blockade of mitochondrial function depends on NCLX. (A) Intracellular sodium content was calculated in murine $CD4^+$ T cells after HS exposure for a period of 30 min (n = 16 from three independent experiments). **(B)** Relative ETC complex II activity under control conditions (CTRL) or in the presence of additional NaCl (+4mM) (n = 3). **(C)** Relative complex II + III activity under increasing concentrations of additional NaCl (+0.0625mM to +64mM) or AA (+0.3438nM to +352nM). **(D)** Relative complex II + III activity was a measured under HS conditions in the presence or absence of NCLX-inhibitor CGP-37157 (CGP). **(E)** Tregs were pre-incubated under HS conditions (+40mM NaCl) in the presence or absence of CGP for 24 h and later co-cultured with CFSE labeled PBMCs at a 1 to 1 ratio. $CD4^+$ Teff proliferation was assessed after 4 days. A FACS plot (left) alongside the percentage proliferation normalized to the HS group is depicted (n = 5 from three independent experiments). **(F)** Ratio between *IFNG* and *IL10* gene expression in Tregs incubated under HS conditions (+40mM NaCl) in the presence or absence of CGP for 72 h (n = 5 from three independent experiments). **(G)** Schematic overview how NCLX controls Treg immunometabolism and function. High sodium environments lead to intracellular Na^+ increases, potentially mediated by NCX[48]. Subsequently, Na^+ could enter in exchange to Ca^{2+} the mitochondria through NCLX. Na^+ inhibits the mitochondrial ETC on the level of complex II/III, resulting in reduced OXPHOS and ATP production. For **(A, B, D, E, and F)** data are depicted as mean ± SEM. *p<0.05, **p<0.01. Normal

distribution was calculated by Shapiro-Wilk normality test with a significance level of 0.05. Significance was calculated by paired two-tailed (**B** and **E**) t test for normal distributed data, by paired one-tailed Wilcoxon test (**F**) for non-normal distributed data, or by unpaired two-tailed (**A**) or one-tailed (**D**) for not normally distributed data. In Na^+ quantifications, outliers were identified with ROUT method and not included in the analysis (**A**).

RESOURCE AVAILABILITY

Lead Contact

Further information and requests for resources should be directed to and will be fulfilled by the Lead Contact, Markus Kleinewietfeld (markus.kleinewietfeld@uhasselt.vib.be).

Materials availability

This study did not generate new unique reagents.

Data and code availability

- Source data for graphs and original western blot images can be found in Data S1. RNA sequencing data have been deposited in NCBI's Gene Expression Omnibus (GEO) database (GSE220530) and are publicly available as of the date of publication. The accession number is provided in the key resources table.
- This paper does not report original code.
- Any additional information required to reanalyze data reported in this paper is available from the lead contact upon request.

EXPERIMENTAL MODEL AND SUBJECT DETAILS

Animal studies were conducted in accordance with the local animal welfare regulations and approved by the respective authorities at the University of Hasselt and University of Regensburg. Mice were kept at the animal facilities in temperature-controlled rooms (21–23 °C) with 12 h light/dark light cycle, with standard food and water provided *ad libitum*. NSG mice were obtained from Charles River, C57BL/6 mice were bred in house. Human peripheral blood samples were obtained from healthy individuals and written informed consent was obtained from all individuals

prior to sample collection. Human studies were approved and conducted in compliance with the institutional review board protocols from Hasselt University (Comité voor Medische Ethiek UHasselt, CME).

METHODS DETAILS

Cell isolation and cell sorting

Human Tregs were isolated as described before[37,41,73] from the peripheral blood of healthy subjects or isolated from buffy coats of healthy donors purchased from the Belgian Red Cross in compliance with institutional review board protocols (CME2019/042 and CME2016/629). In brief, $CD4^+$ T cells were isolated by incubating whole blood with RosetteSep™ Human CD4+ T Cell Enrichment Cocktail (15062, Stemcell) followed by Ficoll-Paque PLUS (GE17-1440-02, Sigma) gradient centrifugation or by using EasySep™ Human $CD4^+$ T Cell Isolation Kit (17952, StemCell). CD25-enriched and -depleted $CD4^+$ cells were isolated with CD25 microbeads II (130-097-044, Miltenyi Biotec). Regulatory T cells (Tregs) were FACS sorted with a FACS Aria II (BD Biosciences) using CD4 APC-Cy7 (clone RPA-T4), CD25 PeCy7 (clone M-A251) and CD127 PerCP-Cy5.5 (clone A019D5). T effector (Teff) cells were isolated by untouched $CD4^+$ T cell isolation (17952, Stemcell) or were FACS sorted for CD25-$CD127^+$ cells. Tregs were isolated according to the following parameters: $CD4^+CD25^{hi}CD127^{low}$ to a FOXP3 purity >96%.

Cell culture, Treg suppression assay and pre-incubation

Human T cells or PBMC were cultured if not otherwise stated in 96-well round-bottom plates (Costar) at $5x10^4$ cells per well in serum-free XVIVO15 (BE02-060F, LONZA) or XVIVO15 medium supplemented with 5% Fetal Bovine Serum (FBS) (S1400, BioWest). Where indicated, T effector cells (Teff) were labelled with CellTrace CFSE (C34554, ThermoFisher Scientific) at 1µM and cultured with fresh or pre-treated Tregs (as indicated in Figure legends) in 96-well round-bottom plates in XVIVO15 medium (LONZA) supplemented with 5% Fetal Bovine Serum. In some cases, Tregs were stained with cell trace violet (CTV) (C34557, ThermoFisher Scientific) at a final concentration of 2.5µM. Cells were stimulated with Treg Inspector beads (αCD2/αCD3/αCD28-coated beads) at 1 bead/cell ratio (130-092-909, Miltenyi Biotec) for 4 to 5 days before analyzed by flow cytometry. When stated, medium was supplemented with additional +40mM NaCl. Tregs

($5x10^4$ cell/well) were stimulated in XVIVO15 medium supplemented with 5% FBS for a period of 6-, 12-, 24-, 72 hours or 4 days in the presence of 1µg/mL of plate-bound αCD3 (clone UCHT1), 1 or 5µg/mL of soluble αCD28 (clone 28.2) and 25U/mL of IL-2 (11147528001, Sigma) in the presence or absence of +40mM NaCl. Where indicated, Tregs were also incubated in the presence of 10µM antimycin A (AA) (A8674, Sigma Aldrich) or 10µM of CGP-37157 (220005, EMD Millipore). After the incubation period, Tregs were removed from culture, washed and used on the different specified assays. DMSO (D2650, Sigma Aldrich) was included as solvent control if necessary.

Generation of monocyte-derived dendritic cells (moDCs)

For monocyte-derived DCs, $CD14^+$ monocytes were magnetically bead-isolated from PBMCs (17858, StemCell Technologies) and cultured with 50U/ml IL-4 (11340045, Immunotools) and 50ng/ml GM-CSF (300-03, Peprotech) in X-VIVO15 supplemented with 10% FBS. After 5 days of incubation, DCs were harvested and stored in liquid nitrogen for later use.

Treg suppression assay using DCs

Treg suppression assays in the presence of DCs were performed as before[37]. Briefly, $CD4^+CD25^-$ Tconvs (referred as Teff) were stained with 1µM Cell Trace CFSE Cell Proliferation Kit (C34554, ThermoFisher Scientific) and cultured with autologous Tregs in 96-well U-bottom plates in X-VIVO15 supplemented with 5% FBS. Cells were stimulated for 4 days using allogenic moDCs in the presence of 0.5ug/mL of soluble αCD3 (555329, BD Bioscience).

Mixed lymphocyte reaction (MLR)

MLR was performed as described before[36]. Briefly, human Treg cells were preincubated under CTRL or HS (+40mM NaCl) conditions with plate bound αCD3, soluble αCD28 and IL-2 for a period of 24 hours. Autologous PBMCs (100 000 cells/well) were stained with CFSE (C34554, ThermoFisher Scientific) and later stimulated with irradiated (3000 rad) allogeneic PBMCs (100 000 cells/well) in RPMI + 10% FCS for 5 days. For suppression of proliferation, pre-incubated autologous Treg cells were added at the indicated ratio.

Murine Treg suppression assay

For murine Treg cell suppression assays, spleens were harvested from 15-week-old C57BL/6J mice. $CD4^+CD25^+$ Treg and $CD4^+CD25^-$ T effector cells (Teff) were isolated using the mouse $CD4^+CD25^+$ Regulatory T Cell Isolation Kit according to the manufacturer's instructions (Miltenyi Biotec #130-091-041, Bergisch Gladbach, Germany). $CD4^+CD25^-$ Teff cells were stained with eF450 Proliferation Dye (Thermo Fisher, Schwerte, Germany). Cells were then cultured at a 1:2, 1:4, 1:8 and 1:16 ratio with 100.000 $CD4^+CD25^-$ Teffs in 96-well plates (Sarstedt, Nümbrecht, Germany) together with 50.000 Treg expansion beads (130-092-909, Miltenyi Biotec) in RPMI1640 medium (Thermo Fisher) in the presence or absence of +40mM NaCl for 4 days.

Flow Cytometry

Cells were analyzed by flow cytometry (FACS) as described before[14] if not specified elsewhere. Duplicates were performed for the different experiments and analysis. Cells were first stained with LIVE/DEAD cell kit (L34972, Invitrogen) or ef780 viabilty dye (Thermo Fisher) to exclude dead cells. For surface staining, cells were labelled with respective antibodies for 15 minutes in MACS buffer (0.5% BSA, 2mM EDTA) at 4°C. For intracellular stainings, cells were first fixed and made permeable using eBioscience™ Foxp3 / Transcription Factor Staining Buffer Set (00-5523-00, Invitrogen) according to manufacturer's instructions and later labelled with respective intracellular antibodies in Perm buffer for 30 minutes at 4°C, washed and assayed in MACS buffer. For cytokine detection, cells were stimulated with 50 ng/ml phorbol12-myristate13-acetate (PMA) (P1585, Sigma) and 250ng/ml Ionomycin (I0634, Sigma) in the presence of GolgiPlug (555029, BD) for 5 hours. Data was acquired on a BD LSR Fortessa II, BD FACS Calibur or BD FACS Canto II and analyzed with FlowJo software (TreeStar).

CRISPR/Cas in human Tregs

CRISPR/Cas technology was applied as done before[41]. Briefly, Tregs were purified by FACS-sorting and expanded for a period of 6 days on 24 well-plates in the presence of 10µg/mL of plate-bound αCD3, 1µg/mL of soluble αCD28 and 300U/mL of IL-2 in XVIVO15 medium supplemented with 5% FBS. On day 6, cells were resuspended in XVIVO15 medium supplemented with 5% FBS and 100U/mL of IL-2 and further incubated in 6 well-plates for a period of 24 hours. For

transfection, cells and RNP mixture was pipetted to a well of a 16-well strip nucleovette (Amaxa™ P3 Primary cell 4D-Nucleofector™ X Kit S V4XP-3032, LONZA) and placed on a 4D-Nucleofector™ (LONZA) using EO115 program. Afterwards, cells were plated in 24-well plates with XVIVO15 medium supplemented with 5% FBS and 100U/mL IL-2. Western blotting was done as described before[14] by using *UQCRFS1* (PA5-21420, ThermoFisher Scientific) and *β-Actin* (3700, Cell signalling) specific antibodies and DNA was isolated as described above for KO determination using Sanger sequencing. Viable KO and control cells were divided into different functional assays. Cells were diluted in RLT buffer for RNA isolation and qRT-PCR analysis, performed as described above. For measuring of suppressive capacity, control (Mock CTRL) and RISP KO Tregs were co-cultured with CFSE-labelled allogeneic total PBMCs on a 1 to 3 ratio in the presence of Treg Inspector beads (αCD2/αCD3/αCD28-coated beads) (130-092-909, Miltenyi Biotec) at 1 bead/cell ratio for 4 days. After incubation, cells were stained and PBMC proliferation was assessed by flow cytometry using a LSR Fortessa II (BD).

Seahorse assays

The metabolic profile was evaluated in 24- and 72 hours cultured Tregs stimulated with αCD3, αCD28 and IL-2, in the presence or absence of +40mM NaCl. Real-time measurements of oxygen consumption rate (OCR) were made using an XF-96 Extracellular Flux Analyzer (Agilent). After incubation times, cells were collected, counted and plated in Cell-tak (354240, Corning) coated XF-96 plates (102416-100, Agilent) at the concentration of 2 x 10^5 cells/well. Cells were let to incubate for 60 min at 37°C, without CO2. A mitochondrial stress test designed to repeat 4 cycles (of 3 minutes mixing followed by 3 minutes measuring) per phase was used to measure OCR under basal conditions and in response to 5μM oligomycin (75351, Sigma Aldrich), 1.5μM of carbonylcyanide-4- (trifluoromethoxy) -phenylhydrazone (FCCP) (C2920, Sigma Aldrich) and 1μM of antimycin A (A8674, Sigma Aldrich) and Rotenone (R8875, Sigma Aldrich).

Phosphorylation analysis

For phosphorylation analysis, Tregs were stimulated as described above for a period of 4 hours in control medium or media supplemented with +40mM NaCl, 10μM antimycin A (AA), 5μM or 200μM of Etomoxir. Controls were incubated in the presence of 100U/mL IL-2 for 30 minutes of

stimulation. Cells were fixed with BD Cytofix™ Fixation Buffer (554655, BD Biosciences) for 10 minutes at 37°C and permeabilized with Perm Buffer III (BD Biosciences, 58050) for 30 minutes on ice. Cells were stained with anti-pSTAT5 antibody (560311, BD Biosciences) for 30 minutes at 4°C and were acquired on a BD LSR Fortessa II.

Determination of intracellular ATP

For ATP rate assays, Tregs were cultured as mentioned before for a period of 6 hours in the presence or absence of +40mM NaCl. Oligomycin A (5μM) was used as a positive control for ATP decrease. ATPlite Luminescence Assay System (6016941, Perkin Elmer) was used for ATP measurements according to the manufacturer's instructions. Briefly, after incubation time, cells were lysed using a cell lysis solution for 5 minutes in constant shaking followed by the addition of a substrate solution. Cells were further incubated for 15 minutes in dark-adapted conditions and luminescence was measured on a FLUOstar OPTIMA reader (BMG Labtech).

Mitochondrial membrane potential measurements

For mitochondrial membrane potential, TMRE-Mitochondrial membrane potential assay kit (ab113852, Abcam) was used according to the manufacturer's instructions. Briefly, Tregs were cultured and activated as described above for a period of 6 hours in the presence or absence of +40mM NaCl and AA (10μM). FCCP (10μM) was used as a positive control and added to the cells 10 minutes before the end of incubation period. After incubation, TMRE was added to the cells and incubated for 20 minutes at 37°C. After, cells were washed and acquired by flow cytometry on a BD Calibur (BD Bioscience).

MitoTracker analysis

To determine mitochondrial content, MitoTracker Green (M7514, ThermoFisher Scientific) was used at a final concentration of 100nM directly into cell culture medium and let to incubate for 60 minutes at 37°C. After, cells were washed in ice-cold PBS (17-516F, LONZA) and further acquired by flow cytometry using a BD LSR Fortessa II.

Electron Transport Chain Complex Assays

The activity of mitochondrial electron transport chain complexes was detected by using different kits. To measure Complex II activity, a Complex II Enzyme activity microplate assay kit (ab109908, Abcam) was performed according to the manufacturer's instructions. Briefly, Tregs were isolated by FACS sorting. Protein extraction was carried using a detergent solution and final concentration was adjusted to recommended dilution for plate loading. Samples were loaded to a 96-well microplate coated with anti-Complex II monoclonal antibody and let to incubate for 2 hours at RT. After, plate was washed, and an activity solution control buffer or buffer containing +4mM NaCl was added to the corresponded wells. Optical density was measured at OD600nm in an iMark Microplate Reader (BIORAD) under kinetic mode for 60 minutes allowing interval measures of 20 seconds. Complex II/III activity was assessed using the MitoTox Complex II+III OXPHOS Activity Assay Kit (ab109905, Abcam) according to the manufacturer's instructions. Activity solution was mixed with increasing concentrations of NaCl (serial dilutions from +64mM to +0.0625mM NaCl) or with AA as positive control (serial dilutions from 352nM to 0.3438nM). Bovine heart mitochondria were added and absorbance at 550nm was measured in kinetic mode on a Spectramax 190 plate reader. Complex II/III activity was calculated relative to the solvent control (water). In some experiments 10μM of CGP-37157 (220005, EMD Millipore) was added.

Mitochondrial ROS measurements

ROS production was assessed on the mitochondria of Tregs using MitoSOX™ Red Mitochondrial Superoxide Indicator kit (M36008, ThermoFisher Scientific) according to the manufacturer's instructions. Briefly, after Tregs incubation for 6 hours in the presence or absence of +40mM NaCl, cells were washed of medium and MitoSOX™ reagent working solution was added and incubated for 10 minutes at 37°C. After, cells were washed and fluorescence was measured by flow cytometry on a BD LSR Fortessa II.

Metabolite extraction and quantification

For metabolite analysis, Tregs were cultured as described above for a period of 12 hours in the presence or absence of +40mM NaCl. Metabolites were extracted on both cells and medium fractions and identified using Liquid chromatography–mass spectrometry (LC-MS). For metabolite extraction on cells, medium was removed and cells washed with ice cold 0.9% NaCl solution.

After, a cellular extraction buffer (80% methanol, containing 2µM d27 myristic acid) was added to the cells and let to incubate for 2-3 minutes on ice. Cells were later centrifuged and supernatant was used for further metabolite identification. Protein pellets were kept in order to determine protein concentration by BCA assay. For medium extraction, 990µL of medium extraction buffer was added to 10µL of medium and stored overnight at -80°C. After incubation, medium samples were centrifuged and supernatants were used for metabolites analysis. Following extraction, the complex mixture of metabolites was separated prior to MS measurement using a Dionex UltiMate 3000 LC System (ThermoFisher Scientific) coupled to a Q Exactive Orbitrap mass spectrometer (ThermoFisher Scientific) operating in negative ion mode. Practically, 10µl of the sample was injected on a C18 column (Aquility UPLC®HSS T3 1.8µm 2.1x100mm). A gradient using solvent A (H2O, 10mM Tributyl-Amine, 15mM acetic acid) and solvent B (100% Methanol) was applied as follows: 0 minutes, 0%B; 2 minutes, 0%B; 7 minutes, 37%B; 14 minutes, 41%B; 26 minutes, 100%B; 30 minutes, 100%B; 31 minutes, 0%B; 40 minutes, 0%B. The flowrate was kept constant at 0.250ml/min and the column was kept at 40°C throughout the analysis. The MS operated in full scan mode (range 70-1050 Th in negative normalized mode) using a spray voltage of 3.2kV, a capillary temperature of 320°C, sheath gas at 50.0, auxiliary gas at 10.0. The AGC target was set at 3e6 using a resolution of 140.000, with a maximum IT of 512ms. Data collection was performed using the Xcalibur software, version 4.2.47 (ThermoFisher Scientific).

Intracellular Na^+ quantification

Mouse (C57BL/6) $CD4^+$ T cells were enriched using $CD4^+$ T cell Isolation Kit (Miltenyi 130-104-454) and incubated for 30 minutes with HS (+10mM or +40mM NaCl) and washed with iso-osmolal sucrose solution. The pellet was lysed with 0.1% Triton and total Na^+ was quantified using an iCE 3000 Series atomic absorption spectrometer (Thermo Scientific) as described before[48]. Animal care and use followed the regulations of the German Animal Welfare Act. The procedures followed were approved by the Umweltamt der Stadt Regensburg and performed in accordance with institutional guidelines.

Transmission electron microscopy

Tregs were cultured as described above in the presence or absence of +40mM NaCl for a period of 6 hours. After incubation, cells were fixed with specific fixative (8% formaldehyde (FA) (EM-grade), 5% glutaraldehyde (GA) (EM-grade), 0.1M Cacodylate buffer) on an equal volume as cells. Cells were fixed for 30 minutes RT in constant rotation. After incubation, fixative was removed and cells were washed 3 times for 30 minutes at 4°C in 0.1M Cacodylate buffer in constant rotation. Once washes were complete, equal volume of 1% Osmium tetroxide (OsO4) was added to the cells and samples were shaken for 1 hour at 4°C. Afterwards, samples were washed by constant shaking for 20 minutes in ddH2O. This step was repeated 4 times. After last washing step, samples were left for 1 hour in 1% Uranyl Acetate (UrAc) under cold and dark conditions for bulk staining. After staining incubation, samples were once again washed by constant shaking in ddH2O for 20 minutes. Washing step was done at 4°C and repeated 4 times. After, samples were dehydrated at 4°C in constant shaking, infiltrated at 4°C and embedding was performed using Spurr's resin. Final step of polymerization was done at 70°C. For the sample sectioning, ultrathin sections of gold interference color made with an ultra-microtome (Leica EM UC6) was performed and post-stained in a Leica EM AC20 for 40 minutes in UrAc at 20°C and for 10 minutes in lead citrate at 20°C. Generated sections were examined and imaged with a JEM 1400plus transmission electron microscope (JEOL, Tokyo, Japan) operating at 80 kV. The 2D transmission electron microscopy images were manually annotated for mitochondria. Cells that were partially visible in the images were omitted from the study. Individual mitochondria were identified with connected component analysis. Morphological features (area, eccentricity, major/minor axis length, and perimeter) were extracted from each mitochondrion. The dimensionality of this feature set was then reduced with U-MAP (https://doi.org/10.21105/joss.00861), which allowed for 2D visualization. The distributions of each feature were compared with kernel density estimation and visualization in violin plots.

RNA isolation and quantitative polymerase chain reaction with reverse transcription (qRT–PCR)

Cells were lysed in RLT buffer (Qiagen) and stored at -80°C until RNA was extracted. For RNA isolation, the Rneasy plus Micro Kit (74034, Qiagen) was used according to the manufacturer's instructions and further converted to cDNA using qScriptTM cDNA SuperMix kit (95048,

QuantaBio) according to manufacturer's instructions. Real Time PCR was performed on a Step ONE Plus RT-PCR machine (Applied Biosciences) using the TaqMan Fast Universal PCR Master Mix (4367846, ThermoFisher Scientific). Primers were purchased from ThermoFisher Scientific (*IL10*- Hs00961622_m1; *CTLA4*- Hs01011591_m1; *IFNG*- Hs00989291_m1; *FOXP3*- Hs01085834_m1) with the exception of *β2M* (4326319E-1402015, Applied Biosystems). Fold-changes in expression were calculated using the ΔΔCT method using human *β2M* as endogenous control for mRNA expression as described before[14]. All fold-changes in the graphs are expressed normalized to the control group.

RNA sequencing (RNAseq)

For RNA sequencing analysis, RNA was isolated as described above. Sequencing libraries were prepared with the NEB Next Ultra DNA Library Prep Kit for Illumina (version 6.0–2/18), according to the manufacturer's protocol including a size selection to 250bp insert size. Sequence-libraries of each sample were equimolarly pooled and sequenced on 4 NextSeq500 v2 flow-cell at 1 × 75 bp (76–8–8–0). Quality of raw sequence reads was checked using FastQC version 0.11.8, and nucleotide calls with a quality score of 28 or higher were considered high quality. Due to low read quality, one sample from the 6 hours control group was removed from analysis. Adapters were removed using cutadapt v.2.4. Reads were aligned to the hg19 genome reference, using STAR (2.5.0e) and a maximum of five mismatches were allowed. Gene counts were retrieved using htseq-count using the "union" option. After removing absent features (zero counts in all samples), the raw counts were imported to R/Bioconductor package DESeq2 v.3.9 to identify differentially expressed genes among samples. The default DESeq2 options were used, including log fold change shrinkage. Differentially expressed genes were considered only when the Benjamini-Hochberg adjusted p-value (false discovery rate [FDR]) was < 0.05. Heatmaps and bar plots were created using the gplots::heatmap.2() and barplot() function respectively on transformed raw counts.

Reanalysis of published transcriptomic datasets

EGAS00001004470[30] were downloaded from the European Genome-phenome Archive (EGA). The quality of raw sequence reads was checked using FastQC version 0.11.8, and the data was analyzed as described above.

Droplet-based single cell (sc)RNAseq preparation

For single cell RNA sequencing (scRNAseq), Tregs were incubated for a period of 6 hours in the presence and absence of +40mM NaCl. After incubation, cells were collected and converted to barcoded scRNAseq libraries by using the Chromium Single Cell 3' Library, Gel Bead & Multiplex Kit and Chip Kit (10x Genomics), aiming for an estimated 5,000 cells per library and following the manufacturer's instructions. Samples were processed using a kit associated to V2 barcoding chemistry of 10x Genomics. Single samples were processed in a single well of a PCR plate, allowing all cells from a sample to be treated with the same master mix and in the same reaction vessel.

scRNAseq profile

RNAseq profiling of single Treg cells was performed with an average sequencing saturation metric of >80%, as calculated by Cell Ranger. Aggregation of sample conditions was done using the Cell Ranger Aggr software from 10x Genomics. Digital gene expression matrices were pre-processed and filtered using the SCRAN and ScaterR packages. Outlier cells were first identified based on three metrics (library size, number of expressed genes and mitochondrial proportion); cells were tagged as outliers when they were four median absolute deviations distant from the median value of each metric across all cells. Secondly, a principal component analysis plot was generated based on the following metrics: 'pct_counts_in_top_100_features', 'total_features_by_ counts', 'pct_counts_feature_control', 'total_features_by_counts_feature_control', 'log10_total_counts_endogenous' and 'log10_total_counts_feature_control'. Outlier cells in this principal component analysis plot were identified using the Rpackage mvoutlier. Low-abundance genes were removed using the 'calcAverage' function and the proposed workflow. The raw counts were normalized and log2 transformed by first calculating 'size factors' that represented the extent to which counts should be scaled in each library. Highly variable genes were detected using the proposed workflow of the scranR package and by applying false discovery rate≤0.05 and

var.out$bio≥0.01 as cutoffs. Highly variable genes were subsequently used for unsupervised dimensionality reduction techniques and principal component analysis. Unsupervised clustering of the cells was performed using graph-based clustering based on SNN-Cliq and PhenoGraph as implemented in the Seurat v.2.3Rpackage (default parameters). Clustering was visualized in two-dimensional scatter plots (via tSNE) using the Seurat v.2.3Rpackage.

Modelling of metabolic pathways based on scRNAseq data

The metabolic landscape of Tregs was modeled using the Compass method (version 0.9.5)[38] by leaving the standard settings unaltered. The gene expression matrix of Tregs single cell data was used as input. The Compass output data was concatenated and transformed as described[38]. To determine which reactions and metabolites were significantly different between groups (CTRL and +40mM NaCl), a Wilcoxon rank sum tests on Compass scores was performed.

Pathway analysis

Ingenuity Pathway Analysis (IPA; Ingenuity Systems/Qiagen) was used to map lists of significant genes (FDR <0.05) to gene ontology groups and biological pathways. The functional and canonical pathway analysis was used to identify the significant biological functions and pathways. Functions and pathways with p-values less than 0.05 (Fischer's exact test) were considered to be statistically significant.

Gene set enrichment analysis

The Gene set enrichment analysis (GSEA) was done using GSEA software (1,2), which uses predefined gene sets from the Molecular Signatures Database (MsigDB). For the present study, we used all the H: hallmark gene sets for GSEA analysis and list of ranked genes based on a score calculated as log10 of p-value multiplied by sign of fold-change. The minimum and maximum criteria for selection of gene sets from the collection were 10 and 500 genes, respectively[74].

Salt-intake in healthy individuals

Daily salt-intake in healthy individuals was assessed as described before[42]. HS and NS intake was defined by a cutoff of >7g/day or <7g/day, respectively. The cohort was comprised of 8 male and 10 female participants with an age range of 35.8±10.4yrs. PBMCs of participants were isolated from peripheral blood and analyzed by FACS as described above.

Experimental autoimmune encephalomyelitis (EAE)

$CD4^+CD25^+$ Treg cells were isolated using the mouse $CD4^+CD25^+$ Regulatory T Cell Isolation Kit according to the manufacturer's instructions (Miltenyi Biotec #130-091-041, Bergisch Gladbach, Germany) from C57BL/6J mice. Cells were plated for 24hrs in 48-well plates (Sarstedt, Nümbrecht, Germany) at 750 thousand cells per well in RPMI 1640 with 10% FCS (both Thermo Fisher) and 2.000 IU/ml recombinant murine IL-2 (Miltenyi Biotec) in the presence or absence of 40mM NaCl or in the presence of 40mM NaCl plus 10µM of CGP-37157 (220005, EMD Millipore). Subsequently, cells were harvested, washed with PBS and adjusted to one million cells/ml in PBS. Cells were injected intravenously (i.v) (500 thousand cells/mouse) at day 6 of EAE. Active EAE was induced by immunizing 12-week-old female, in house bred C57BL/6J mice with 200 µg MOG (35-55, Charité, Berlin, Germany) in 200 µg CFA (BD) subcutaneously at the flanks and tail base. 200 ng of pertussis toxin (PTX) (List, Campbell, CA) were applied intraperitoneally (i.p) on days 0 and 2 post immunization. Animals were weighted and scored on a daily basis. Scores were as follows: 1- limp tail, 2- gait ataxia, 3- paraparesis, 4- tetraparesis, 5- moribund or death. All animal experiments were performed in accordance with the local animal welfare regulations and approved by the respective authorities (AZ: 55.2.2-2532-2.1293-29).

Xenogeneic graft versus host disease (xGvHD)

Six- to ten-week-old male NSG mice were purchased from Charles River and housed randomly on different IVC cages at the in-house animal care facility. Mice received autoclaved chow and tap water *ad libitum* for 9 days before induction. For xGvHD induction, each animal received $1.3x10^7$ CD25-depleted PBMCs alone (PBMC group) or together with 0.2x107 CD25-enriched Tregs pre-activated with αCD3 (1µg/mL), αCD28 (1µg/mL) and IL-2 (25U/mL) for 6 hours in control media or media supplemented with +40mM NaCl (HS group) or in media containing 10µM of antimycin A (AA group) or in media supplemented with +40mM NaCl containing 10µM of CGP-

37157 (CGP group). After thorough washing, cells were resuspended in PBS and injected through the tail vein. The weight and clinical symptoms of the mice were monitored during the entire course of the experiment. Clinical symptoms were scored according to general appearance and mobility as described before[15]. At sacrifice, organs were collected, processed and cells were used for FACS. Engraftment of human cells was monitored by FACS analysis of peripheral blood.

Study approval

Human studies were conducted in compliance with the institutional review board protocols from Hasselt University (CME2019/042, CME2016/629 and UH-SALTMS-P1). If not mentioned elsewhere, animal studies were approved by the ethics committee of animal studies at the University of Hasselt (ID 201739).

Quantification and statistical analysis

Statistical analyses were performed with GraphPad Prism Version 8. All data were presented as mean ± SEM, unless stated otherwise. Value of n is always displayed in the Figure as individual data point, referring to an independent biological replicate, more information about absolute n numbers can be found in the Figure legends. All statistical test used were also indicated in the respective Figure legends. Normality of the data was tested by Shapiro-Wilk normality test. Significance between two groups was analyzed by t-test (when normal distributed) or Wilcoxon matched-pairs signed rank test (for non-normal distributed). For more than two groups with one variable only, one-way ANOVA with Tukey's post-hoc test (for normal distributed data) was used. Matched data with more than two groups (or time points) was analyzed by Friedman test and FDR-correction was performed via Benjamini-Hochberg procedure or Holm Sidak's multiple comparison tests. For the survival analysis of the *in vivo* data, a curve comparison test with Mantel-Cox and Gehan-Breslow-Wilcoxon test was applied. Exact statistical tests used are described in the respective Figure legends. Respective p-values were depicted in the figures and legends.

Table I. Key resources table

REAGENT or RESOURCE	SOURCE	IDENTIFIER
Antibodies		

Alexa647 CCR6 anti-human	BD Biosciences	Cat# 560466
APC IL10 anti-human	BD Biosciences	Cat# 554707
APC CD4 anti-mouse	Biolegend	Cat# 100516
APC-Cy7 CD4 anti-human	BD Biosciences	Cat# 557871
AF488 HELIOS anti-human	BD Biosciences	Cat# 563950
AF700 FOXP3 anti-human	eBioscience	Cat# 56-4776-41
BV605 CD8 anti-human	BD Biosciences	Cat# 740411
BV605 TIGIT anti-human	Biolegend	Cat# 372712
BV650 CD45 anti-mouse	BD Biosciences	Cat# 563410
BV786 CD39 anti-human	BD Biosciences	Cat# 742523
CD3 anti-human	BD Biosciences	Cat# 555329
CD28 anti-human	BD Biosciences	Cat# 302933
eF450 Proliferation dye	eBioscience	Cat# 65-0842-90
eF506 CD3 anti-human	Invitrogen by ThermoFisher Scientific	Cat# 69-0038-42
eF780 Viability dye	eBioscience	Cat# 65-0865-18
FITC HLA-DR anti-human	BD Biosciences	Cat# 347363
Pacific blue CD3 anti-human	Biolegend	Cat# 317314
Pacific blue pSTAT5 anti-human	BD Biosciences	Cat# 560311
PE CD44 anti-mouse	Biolegend	Cat# 103008
PE CTLA4 anti-human	BD Biosciences	Cat# 555853
PE FOXP3 anti-human	Biolegend	Cat# 320008
PE IL10 anti-human	BD Biosciences	Cat# 559330
PeCy7 CD25 anti-human	BD Biosciences	Cat# 557741
PeCy7 IFN-γ anti-human	eBioscience	Cat# 25-7319-82
PercP-Cy5.5 CD127 anti-human	Biolegend	Cat# 351322
Biological Samples		
Human peripheral blood mononuclear cells	In-house	N/A
Buffy coats	Belgium Red Cross	N/A
Chemicals, Peptides, and Recombinant Proteins		
Antimycin A	Sigma-Aldrich	Cat# A8674
BD Cytofix™ Fixation Buffer	BD Biosciences	Cat# 554655

BD FACSClean	BD Biosciences	Cat# 340345
BD FACSFlow	BD Biosciences	Cat# 342003
BD FACSRinse	BD Biosciences	Cat# 340346
Beta-mercaptoethanol	Sigma-Aldrich	Cat# M3148
Bovine Serum Albumin (BSA)	Sigma-Aldrich	Cat# A2153
Carbonyl cyanide 4-(trifluoromethoxy)phenylhydrazone (FCCP)	Sigma-Aldrich	Cat# C2920
Carboxy-DCFDA (5-(and-6)-Carboxy-2',7'-Dichlorofluorescein Diacetate)	ThermoFisher Scientific	Cat# C369
Cas9	Aldevron	Cat# 9212
CellTrace™ CFSE Cell Proliferation Kit, for flow cytometry	ThermoFisher Scientific	Cat# C34554
CellTrace™ Violet Cell Proliferation Kit, for flow cytometry	ThermoFisher Scientific	Cat# C34557
CGP-37157	EMD Millipore	Cat# 220005
Complete Freunds Adjuvant (CFA)	BD	Cat# 210485
DMEM without glucose, L-glutamine, phenol red, sodium pyruvate and sodium bicarbonate, powder	Sigma-Aldrich	Cat# D5030
Dimethylsulfoxide (DMSO)	Sigma-Aldrich	Cat# D2650
eBioscience™ Foxp3 / Transcription Factor Staining Buffer Set	Invitrogen by ThermoFisher Scientific	Cat# 00-5523-00
Ethylenediaminetetraacetic acid (EDTA)	ThermoFisher Scientific	Cat# 15575020
Fetal bovine serum	Biowest	Cat# S1400
Ficoll Paque PLUS	Sigma-Aldrich	Cat# GE17-1440-02
Glucose (D(+)-)	Sigma-Aldrich	Cat# G8270
Glutamax 100x	ThermoFisher Scientific	Cat# 35050061
GM-CSF, human	Peprotech	Cat# 300-03
IL-2, human	Sigma-Aldrich	Cat# 11147528001
IL-4, human	Immunotools	Cat# 11340045
MitoTracker Green FM	ThermoFisher Scientific	Cat# M7514
MOG 35-55	Charité, Berlin	N/A
Oligomycin A	Sigma-Aldrich	Cat# 75351
P3 Primary cell 4D Nucleofector™ X kit S	LONZA	Cat# V4XP-3032
Perm Buffer III	BD Biosciences	Cat# 558050
Pertussis toxin (PTX)	List Labs	Cat# 180

PBS	LONZA	Cat# 17-516F
RBC lysis buffer (10x)	ThermoFisher Scientific	Cat# 00-4300-54
Recombinant murine IL-2	Miltenyi Biotec	Cat# 130-120-662
Rotenone	Sigma-Aldrich	Cat# R8875
RPMI medium	Gibco by Thermo Fisher Scientific	Cat# 11875085
Sodium chloride	VWR	Cat# 27810.364
Sodium pyruvate	Gibco by Thermo Fisher Scientific	Cat# 11360070
Sucrose	Sigma	Cat# S0389
TaqMan fast universal PCR master mix 2x	Applied Biosystems by Thermo Fisher Scientific	Cat# 4367846
Triton X-100	Sigma	Cat# T9284
Trypan blue 0.5%	PromoCell	Cat# PK-CA902-1209
X-VIVO 15 media	Lonza	Cat# BE02-060F
Critical Commercial Assays		
ATPlite Luminescence Assay System	PerkinElmer	Cat# 6016941
Complex II Enzyme Activity Microplate Assay Kit	Abcam	Cat# ab109908
$CD4^+CD25^+$ Regulatory T Cell Isolation Kit	Miltenyi Biotec	Cat# 130-091-041
CD25 microbeads II, Human lyophilized	Miltenyi Biotec	Cat# 130-097-044
Chromium Single Cell 3' Library & Gel Bead Kit v2, 16 rxns	10x Genomics	Cat# PN-120237
Chromium Single Cell A Chip Kit, 16 rxns	10x Genomics	Cat# PN-1000009
Chromium i7 Multiplex Kit, 96 rxns	10x Genomics	Cat# PN-120262
EasySep $CD4^+$ T cell isolation kit human	Stemcell Technologies	Cat# 17952
EasySep™ Human CD14 Positive Selection Kit II	Stemcell Technologies	Cat# 17858
Human Treg suppression Inspector beads	Miltenyi Biotec	Cat# 130-092-909
LIVE/DEAD® Fixable Red Dead Cell Stain Kit, for 488nm excitation	Invitrogen by Thermo Fisher Scientific	Cat# L34972
MitoSOX™ Red Mitochondrial Superoxide Indicator, for live-cell imaging	ThermoFisher Scientific	Cat# M36008
MitoTox Complex II + III OXPHOS Activity Assay Kit	Abcam	Cat# ab109905
qScript cDNA SuperMix	Quanta Biosciences	Cat# 95048
RNeasy Plus Micro Kit	Qiagen	Cat# 74034
RosetteSep™ Human CD4+ T Cell Enrichment Cocktail	Stemcell Technologies	Cat# 15062

Seahorse Xfe96 FluxPak	Agilent	Cat# 102416-100
TMRE-Mitochondrial Membrane Potential Assay Kit	Abcam	Cat# ab113852
Treg expansion kit, mouse	Miltenyi Biotec	Cat# 130-095-925
Deposited data		
RNA sequencing data	This study	GEO: GSE220530
Data S1	This study	N/A
Experimental Models: Organisms/Strains		
NOD.Cg-*Prkdc*^{scid} *Il2rg*^{tm1Wjl}/SzJ (NSG) mice, 8- to 10-week-old, male	Charles-River	Strain code: 614
C57BL/6J mice, 9- to 15-week-old, female	In-house	N/A
Oligonucleotides		
RISP gRNA CAAGAGAAAGCAGCGAGGCT	Synthego	N/A
Software and Algorithms		
BD FACSDiva	BD Biosciences	N/A
BioRender	BioRender	N/A
Cell Ranger	10x Genomics	N/A
FlowJo 10.5.3	Tree Star by BD Biosciences	N/A
GSEA 4.0.3	Broad Institute	N/A
Ingenuity Pathway Analysis Software	Qiagen	N/A
Prism Version 8	GraphPad	N/A
QuPath 0.2.0	University of Edinburgh.	N/A
R 3.5.1	GNU General Public License	N/A
RStudio	GNU General Public License	N/A
Wave 2.6.0.31	Agilent Technologies	N/A

REFERENCES

1. Kleinewietfeld, M., and Hafler, D.A. (2014). Regulatory T cells in autoimmune neuroinflammation. Immunol. Rev. *259*, 231-244. 10.1111/imr.12169.
2. Sakaguchi, S., Miyara, M., Costantino, C.M., and Hafler, D.A. (2010). FOXP3+ regulatory T cells in the human immune system. Nat. Rev. Immunol. *10*, 490-500. 10.1038/nri2785.

3. Arroyo Hornero, R., Hamad, I., Côrte-Real, B., and Kleinewietfeld, M. (2020). The Impact of Dietary Components on Regulatory T Cells and Disease. Front. Immunol. *11*, 253. 10.3389/fimmu.2020.00253.

4. Hatzioannou, A., Boumpas, A., Papadopoulou, M., Papafragkos, I., Varveri, A., Alissafi, T., and Verginis, P. (2021). Regulatory T Cells in Autoimmunity and Cancer: A Duplicitous Lifestyle. Front. Immunol. *12*, 731947. 10.3389/fimmu.2021.731947.

5. Overacre-Delgoffe, A.E., and Vignali, D.A.A. (2018). Treg Fragility: A Prerequisite for Effective Antitumor Immunity? Cancer Immunol Res *6*, 882-887. 10.1158/2326-6066.CIR-18-0066.

6. Kleinewietfeld, M., and Hafler, D.A. (2013). The plasticity of human Treg and Th17 cells and its role in autoimmunity. Semin. Immunol. *25*, 305-312. 10.1016/j.smim.2013.10.009.

7. Overacre-Delgoffe, A.E., Chikina, M., Dadey, R.E., Yano, H., Brunazzi, E.A., Shayan, G., Horne, W., Moskovitz, J.M., Kolls, J.K., Sander, C., et al. (2017). Interferon-gamma Drives Treg Fragility to Promote Anti-tumor Immunity. Cell *169*, 1130-1141 e1111. 10.1016/j.cell.2017.05.005.

8. Dominguez-Villar, M., and Hafler, D.A. (2018). Regulatory T cells in autoimmune disease. Nat. Immunol. *19*, 665-673. 10.1038/s41590-018-0120-4.

9. Junius, S., Mavrogiannis, A.V., Lemaitre, P., Gerbaux, M., Staels, F., Malviya, V., Burton, O., Gergelits, V., Singh, K., Tito Tadeo, R.Y., et al. (2021). Unstable regulatory T cells, enriched for naive and Nrp1(neg) cells, are purged after fate challenge. Sci Immunol *6*. 10.1126/sciimmunol.abe4723.

10. Saxena, V., Lakhan, R., Iyyathurai, J., and Bromberg, J.S. (2021). Mechanisms of exTreg induction. Eur. J. Immunol. *51*, 1956-1967. 10.1002/eji.202049123.

11. Müller, D.N., Wilck, N., Haase, S., Kleinewietfeld, M., and Linker, R.A. (2019). Sodium in the microenvironment regulates immune responses and tissue homeostasis. Nat. Rev. Immunol. *19*, 243-254. 10.1038/s41577-018-0113-4.

12. Manzel, A., Muller, D.N., Hafler, D.A., Erdman, S.E., Linker, R.A., and Kleinewietfeld, M. (2014). Role of "Western diet" in inflammatory autoimmune diseases. Curr. Allergy Asthma Rep. *14*, 404. 10.1007/s11882-013-0404-6.

13. Wu, C., Yosef, N., Thalhamer, T., Zhu, C., Xiao, S., Kishi, Y., Regev, A., and Kuchroo, V.K. (2013). Induction of pathogenic TH17 cells by inducible salt-sensing kinase SGK1. Nature *496*, 513-517. 10.1038/nature11984.

14. Kleinewietfeld, M., Manzel, A., Titze, J., Kvakan, H., Yosef, N., Linker, R.A., Muller, D.N., and Hafler, D.A. (2013). Sodium chloride drives autoimmune disease by the induction of pathogenic TH17 cells. Nature *496*, 518-522. 10.1038/nature11868.

15. Hernandez, A.L., Kitz, A., Wu, C., Lowther, D.E., Rodriguez, D.M., Vudattu, N., Deng, S., Herold, K.C., Kuchroo, V.K., Kleinewietfeld, M., and Hafler, D.A. (2015). Sodium chloride inhibits the suppressive function of FOXP3+ regulatory T cells. J. Clin. Invest. *125*, 4212-4222. 10.1172/jci81151.

16. Sumida, T., Lincoln, M.R., Ukeje, C.M., Rodriguez, D.M., Akazawa, H., Noda, T., Naito, A.T., Komuro, I., Dominguez-Villar, M., and Hafler, D.A. (2018). Activated β-catenin in Foxp3(+) regulatory T cells links inflammatory environments to autoimmunity. Nat. Immunol. *19*, 1391-1402. 10.1038/s41590-018-0236-6.

17. Safa, K., Ohori, S., Borges, T.J., Uehara, M., Batal, I., Shimizu, T., Magee, C.N., Belizaire, R., Abdi, R., Wu, C., et al. (2015). Salt Accelerates Allograft Rejection through Serum- and Glucocorticoid-Regulated Kinase-1-Dependent Inhibition of Regulatory T Cells. J. Am. Soc. Nephrol. *26*, 2341-2347. 10.1681/ASN.2014090914.

18. Yang, Y.H., Istomine, R., Alvarez, F., Al-Aubodah, T.A., Shi, X.Q., Takano, T., Thornton, A.M., Shevach, E.M., Zhang, J., and Piccirillo, C.A. (2020). Salt Sensing by Serum/Glucocorticoid-Regulated Kinase 1 Promotes Th17-like Inflammatory Adaptation of Foxp3(+) Regulatory T Cells. Cell Rep. *30*, 1515-1529.e1514. 10.1016/j.celrep.2020.01.002.

19. Luo, Y., Xue, Y., Wang, J., Dang, J., Fang, Q., Huang, G., Olsen, N., and Zheng, S.G. (2019). Negligible Effect of Sodium Chloride on the Development and Function of TGF-β-Induced CD4(+) Foxp3(+) Regulatory T Cells. Cell Rep. *26*, 1869-1879.e1863. 10.1016/j.celrep.2019.01.066.

20. Geltink, R.I.K., Kyle, R.L., and Pearce, E.L. (2018). Unraveling the Complex Interplay Between T Cell Metabolism and Function. Annu. Rev. Immunol. *36*, 461-488. 10.1146/annurev-immunol-042617-053019.

21. Norata, G.D., Caligiuri, G., Chavakis, T., Matarese, G., Netea, M.G., Nicoletti, A., O'Neill, L.A., and Marelli-Berg, F.M. (2015). The Cellular and Molecular Basis of Translational Immunometabolism. Immunity *43*, 421-434. 10.1016/j.immuni.2015.08.023.

22. Newton, R., Priyadharshini, B., and Turka, L.A. (2016). Immunometabolism of regulatory T cells. Nat. Immunol. *17*, 618-625. 10.1038/ni.3466.

23. Chapman, N.M., Boothby, M.R., and Chi, H. (2020). Metabolic coordination of T cell quiescence and activation. Nat. Rev. Immunol. *20*, 55-70. 10.1038/s41577-019-0203-y.

24. Binger, K.J., Côrte-Real, B.F., and Kleinewietfeld, M. (2017). Immunometabolic Regulation of Interleukin-17-Producing T Helper Cells: Uncoupling New Targets for Autoimmunity. Front. Immunol. *8*, 311. 10.3389/fimmu.2017.00311.

25. Kurniawan, H., Franchina, D.G., Guerra, L., Bonetti, L., Baguet, L.S., Grusdat, M., Schlicker, L., Hunewald, O., Dostert, C., Merz, M.P., et al. (2020). Glutathione Restricts Serine Metabolism to Preserve Regulatory T Cell Function. Cell Metab. *31*, 920-936.e927. 10.1016/j.cmet.2020.03.004.

26. Pompura, S.L., Wagner, A., Kitz, A., Laperche, J., Yosef, N., Dominguez-Villar, M., and Hafler, D. (2020). Oleic acid restores suppressive defects in tissue-resident FOXP3 regulatory T cells from patients with multiple sclerosis. J. Clin. Invest. 10.1172/JCI138519.

27. Weinberg, S.E., Singer, B.D., Steinert, E.M., Martinez, C.A., Mehta, M.M., Martínez-Reyes, I., Gao, P., Helmin, K.A., Abdala-Valencia, H., Sena, L.A., et al. (2019). Mitochondrial complex III is essential for suppressive function of regulatory T cells. Nature *565*, 495-499. 10.1038/s41586-018-0846-z.

28. Duscha, A., Gisevius, B., Hirschberg, S., Yissachar, N., Stangl, G.I., Eilers, E., Bader, V., Haase, S., Kaisler, J., David, C., et al. (2020). Propionic Acid Shapes the Multiple Sclerosis Disease Course by an Immunomodulatory Mechanism. Cell *180*, 1067-1080.e1016. 10.1016/j.cell.2020.02.035.

29. La Rocca, C., Carbone, F., De Rosa, V., Colamatteo, A., Galgani, M., Perna, F., Lanzillo, R., Brescia Morra, V., Orefice, G., Cerillo, I., et al. (2017). Immunometabolic profiling of T cells from patients with relapsing-remitting multiple sclerosis reveals an impairment in

glycolysis and mitochondrial respiration. Metabolism *77*, 39-46. 10.1016/j.metabol.2017.08.011.

30. Alissafi, T., Kalafati, L., Lazari, M., Filia, A., Kloukina, I., Manifava, M., Lim, J.H., Alexaki, V.I., Ktistakis, N.T., Doskas, T., et al. (2020). Mitochondrial Oxidative Damage Underlies Regulatory T Cell Defects in Autoimmunity. Cell Metab. 10.1016/j.cmet.2020.07.001.

31. Hernansanz-Agustin, P., Choya-Foces, C., Carregal-Romero, S., Ramos, E., Oliva, T., Villa-Pina, T., Moreno, L., Izquierdo-Alvarez, A., Cabrera-Garcia, J.D., Cortes, A., et al. (2020). Na(+) controls hypoxic signalling by the mitochondrial respiratory chain. Nature. 10.1038/s41586-020-2551-y.

32. Geisberger, S., Bartolomaeus, H., Neubert, P., Willebrand, R., Zasada, C., Bartolomaeus, T., McParland, V., Swinnen, D., Geuzens, A., Maifeld, A., et al. (2021). Salt Transiently Inhibits Mitochondrial Energetics in Mononuclear Phagocytes. Circulation. 10.1161/CIRCULATIONAHA.120.052788.

33. Wiig, H., Schröder, A., Neuhofer, W., Jantsch, J., Kopp, C., Karlsen, T.V., Boschmann, M., Goss, J., Bry, M., Rakova, N., et al. (2013). Immune cells control skin lymphatic electrolyte homeostasis and blood pressure. J. Clin. Invest. *123*, 2803-2815. 10.1172/JCI60113.

34. Machnik, A., Neuhofer, W., Jantsch, J., Dahlmann, A., Tammela, T., Machura, K., Park, J.K., Beck, F.X., Müller, D.N., Derer, W., et al. (2009). Macrophages regulate salt-dependent volume and blood pressure by a vascular endothelial growth factor-C-dependent buffering mechanism. Nat. Med. *15*, 545-552. 10.1038/nm.1960.

35. Jantsch, J., Schatz, V., Friedrich, D., Schroder, A., Kopp, C., Siegert, I., Maronna, A., Wendelborn, D., Linz, P., Binger, K.J., et al. (2015). Cutaneous Na+ storage strengthens the antimicrobial barrier function of the skin and boosts macrophage-driven host defense. Cell Metab. *21*, 493-501. 10.1016/j.cmet.2015.02.003.

36. Kleinewietfeld, M., Starke, M., Di Mitri, D., Borsellino, G., Battistini, L., Rotzschke, O., and Falk, K. (2009). CD49d provides access to "untouched" human Foxp3+ Treg free of contaminating effector cells. Blood *113*, 827-836. 10.1182/blood-2008-04-150524.

37. Arroyo-Hornero, R., Aegerter, H., Hamad, I., Corte-Real, B., Staes, K., van der Woning, B., Verstraete, K., Savvides, S.N., Lambrecht, B.N., and Kleinewietfeld, M. (2022). The

Charcot-Leyden Crystal protein Galectin-10 is not a major determinant of human regulatory T cell function. Allergy. 10.1111/all.15332.

38. Wagner, A., Wang, C., Fessler, J., DeTomaso, D., Avila-Pacheco, J., Kaminski, J., Zaghouani, S., Christian, E., Thakore, P., Schellhaass, B., et al. (2021). Metabolic modeling of single Th17 cells reveals regulators of autoimmunity. Cell *184*, 4168-4185 e4121. 10.1016/j.cell.2021.05.045.

39. Nastasi, C., Willerlev-Olsen, A., Dalhoff, K., Ford, S.L., Gadsboll, A.O., Buus, T.B., Gluud, M., Danielsen, M., Litman, T., Bonefeld, C.M., et al. (2021). Inhibition of succinate dehydrogenase activity impairs human T cell activation and function. Sci. Rep. *11*, 1458. 10.1038/s41598-020-80933-7.

40. Howie, D., Cobbold, S.P., Adams, E., Ten Bokum, A., Necula, A.S., Zhang, W., Huang, H., Roberts, D.J., Thomas, B., Hester, S.S., et al. (2017). Foxp3 drives oxidative phosphorylation and protection from lipotoxicity. JCI Insight *2*, e89160. 10.1172/jci.insight.89160.

41. Van Zeebroeck, L., Arroyo Hornero, R., Côrte-Real, B.F., Hamad, I., Meissner, T.B., and Kleinewietfeld, M. (2021). Fast and Efficient Genome Editing of Human FOXP3+ Regulatory T Cells. Front. Immunol. *12*. 10.3389/fimmu.2021.655122.

42. Mahler, A., Klamer, S., Maifeld, A., Bartolomaeus, H., Marko, L., Chen, C.Y., Forslund, S.K., Boschmann, M., Muller, D.N., and Wilck, N. (2022). Increased Salt Intake Decreases Diet-Induced Thermogenesis in Healthy Volunteers: A Randomized Placebo-Controlled Study. Nutrients *14*. 10.3390/nu14020253.

43. Zhang, X., Koldzic, D.N., Izikson, L., Reddy, J., Nazareno, R.F., Sakaguchi, S., Kuchroo, V.K., and Weiner, H.L. (2004). IL-10 is involved in the suppression of experimental autoimmune encephalomyelitis by CD25+CD4+ regulatory T cells. Int. Immunol. *16*, 249-256. 10.1093/intimm/dxh029.

44. Kohm, A.P., Carpentier, P.A., Anger, H.A., and Miller, S.D. (2002). Cutting edge: CD4+CD25+ regulatory T cells suppress antigen-specific autoreactive immune responses and central nervous system inflammation during active experimental autoimmune encephalomyelitis. J. Immunol. *169*, 4712-4716. 10.4049/jimmunol.169.9.4712.

45. Hahn, S.A., Bellinghausen, I., Trinschek, B., and Becker, C. (2015). Translating Treg Therapy in Humanized Mice. Front. Immunol. *6*, 623. 10.3389/fimmu.2015.00623.

46. Guichelaar, T., Emmelot, M.E., Rozemuller, H., Martini, B., Groen, R.W., Storm, G., Lokhorst, H.M., Martens, A.C., and Mutis, T. (2013). Human regulatory T cells do not suppress the antitumor immunity in the bone marrow: a role for bone marrow stromal cells in neutralizing regulatory T cells. Clin Cancer Res *19*, 1467-1475. 10.1158/1078-0432.ccr-12-2177.

47. Mutis, T., van Rijn, R.S., Simonetti, E.R., Aarts-Riemens, T., Emmelot, M.E., van Bloois, L., Martens, A., Verdonck, L.F., and Ebeling, S.B. (2006). Human regulatory T cells control xenogeneic graft-versus-host disease induced by autologous T cells in RAG2-/-gammac-/- immunodeficient mice. Clin Cancer Res *12*, 5520-5525. 10.1158/1078-0432.ccr-06-0035.

48. Neubert, P., Homann, A., Wendelborn, D., Bar, A.L., Krampert, L., Trum, M., Schroder, A., Ebner, S., Weichselbaum, A., Schatz, V., et al. (2020). NCX1 represents an ionic Na+ sensing mechanism in macrophages. PLoS Biol. *18*, e3000722. 10.1371/journal.pbio.3000722.

49. Neubert, P., Schröder, A., Müller, D.N., and Jantsch, J. (2019). Interplay of Na(+) Balance and Immunobiology of Dendritic Cells. Front. Immunol. *10*, 599. 10.3389/fimmu.2019.00599.

50. Ait-Oufella, H., Salomon, B.L., Potteaux, S., Robertson, A.K., Gourdy, P., Zoll, J., Merval, R., Esposito, B., Cohen, J.L., Fisson, S., et al. (2006). Natural regulatory T cells control the development of atherosclerosis in mice. Nat. Med. *12*, 178-180. 10.1038/nm1343.

51. Kvakan, H., Kleinewietfeld, M., Qadri, F., Park, J.K., Fischer, R., Schwarz, I., Rahn, H.P., Plehm, R., Wellner, M., Elitok, S., et al. (2009). Regulatory T cells ameliorate angiotensin II-induced cardiac damage. Circulation *119*, 2904-2912. 10.1161/CIRCULATIONAHA.108.832782.

52. Weirather, J., Hofmann, U.D., Beyersdorf, N., Ramos, G.C., Vogel, B., Frey, A., Ertl, G., Kerkau, T., and Frantz, S. (2014). Foxp3+ CD4+ T cells improve healing after myocardial infarction by modulating monocyte/macrophage differentiation. Circ. Res. *115*, 55-67. 10.1161/CIRCRESAHA.115.303895.

53. Meng, X., Yang, J., Dong, M., Zhang, K., Tu, E., Gao, Q., Chen, W., Zhang, C., and Zhang, Y. (2016). Regulatory T cells in cardiovascular diseases. Nat. Rev. Cardiol. *13*, 167-179. 10.1038/nrcardio.2015.169.

54. Baardman, J., and Lutgens, E. (2020). Regulatory T Cell Metabolism in Atherosclerosis. Metabolites *10*. 10.3390/metabo10070279.

55. Saigusa, R., Winkels, H., and Ley, K. (2020). T cell subsets and functions in atherosclerosis. Nat. Rev. Cardiol. *17*, 387-401. 10.1038/s41569-020-0352-5.

56. Tang, A.S., Wells, G.A., Talajic, M., Arnold, M.O., Sheldon, R., Connolly, S., Hohnloser, S.H., Nichol, G., Birnie, D.H., Sapp, J.L., et al. (2010). Cardiac-resynchronization therapy for mild-to-moderate heart failure. N. Engl. J. Med. *363*, 2385-2395. 10.1056/NEJMoa1009540.

57. Butcher, M.J., Filipowicz, A.R., Waseem, T.C., McGary, C.M., Crow, K.J., Magilnick, N., Boldin, M., Lundberg, P.S., and Galkina, E.V. (2016). Atherosclerosis-Driven Treg Plasticity Results in Formation of a Dysfunctional Subset of Plastic IFNgamma+ Th1/Tregs. Circ. Res. *119*, 1190-1203. 10.1161/CIRCRESAHA.116.309764.

58. Bansal, S.S., Ismahil, M.A., Goel, M., Zhou, G., Rokosh, G., Hamid, T., and Prabhu, S.D. (2019). Dysfunctional and Proinflammatory Regulatory T-Lymphocytes Are Essential for Adverse Cardiac Remodeling in Ischemic Cardiomyopathy. Circulation *139*, 206-221. 10.1161/CIRCULATIONAHA.118.036065.

59. He, W., Xu, J., Mu, R., Li, Q., Lv, D.L., Huang, Z., Zhang, J., Wang, C., and Dong, L. (2020). High-salt diet inhibits tumour growth in mice via regulating myeloid-derived suppressor cell differentiation. Nat Commun *11*, 1732. 10.1038/s41467-020-15524-1.

60. Willebrand, R., Hamad, I., Van Zeebroeck, L., Kiss, M., Bruderek, K., Geuzens, A., Swinnen, D., Côrte-Real, B.F., Markó, L., Lebegge, E., et al. (2019). High Salt Inhibits Tumor Growth by Enhancing Anti-tumor Immunity. Front. Immunol. *10*, 1141. 10.3389/fimmu.2019.01141.

61. Binger, K.J., Gebhardt, M., Heinig, M., Rintisch, C., Schroeder, A., Neuhofer, W., Hilgers, K., Manzel, A., Schwartz, C., Kleinewietfeld, M., et al. (2015). High salt reduces the activation of IL-4- and IL-13-stimulated macrophages. J. Clin. Invest. *125*, 4223-4238. 10.1172/JCI80919.

62. Ip, W.K., and Medzhitov, R. (2015). Macrophages monitor tissue osmolarity and induce inflammatory response through NLRP3 and NLRC4 inflammasome activation. Nat Commun *6*, 6931. 10.1038/ncomms7931.

63. Boyman, L., Williams, G.S., Khananshvili, D., Sekler, I., and Lederer, W.J. (2013). NCLX: the mitochondrial sodium calcium exchanger. J. Mol. Cell. Cardiol. *59*, 205-213. 10.1016/j.yjmcc.2013.03.012.

64. Czyz, A., and Kiedrowski, L. (2003). Inhibition of plasmalemmal Na(+)/Ca(2+) exchange by mitochondrial Na(+)/Ca(2+) exchange inhibitor 7-chloro-5-(2-chlorophenyl)-1,5-dihydro-4,1-benzothiazepin-2(3H)-one (CGP-37157) in cerebellar granule cells. Biochem. Pharmacol. *66*, 2409-2411. 10.1016/j.bcp.2003.08.024.

65. Tanaka, H., Nishimaru, K., Aikawa, T., Hirayama, W., Tanaka, Y., and Shigenobu, K. (2002). Effect of SEA0400, a novel inhibitor of sodium-calcium exchanger, on myocardial ionic currents. Br. J. Pharmacol. *135*, 1096-1100. 10.1038/sj.bjp.0704574.

66. Liu, T., Takimoto, E., Dimaano, V.L., DeMazumder, D., Kettlewell, S., Smith, G., Sidor, A., Abraham, T.P., and O'Rourke, B. (2014). Inhibiting mitochondrial Na+/Ca2+ exchange prevents sudden death in a Guinea pig model of heart failure. Circ. Res. *115*, 44-54. 10.1161/CIRCRESAHA.115.303062.

67. Luongo, T.S., Lambert, J.P., Gross, P., Nwokedi, M., Lombardi, A.A., Shanmughapriya, S., Carpenter, A.C., Kolmetzky, D., Gao, E., van Berlo, J.H., et al. (2017). The mitochondrial Na(+)/Ca(2+) exchanger is essential for Ca(2+) homeostasis and viability. Nature *545*, 93-97. 10.1038/nature22082.

68. Martinez-Sanz, F.J., Lajarin-Cuesta, R., Gonzalez-Lafuente, L., Moreno-Ortega, A.J., Punzon, E., Cano-Abad, M.F., and de los Rios, C. (2016). Neuroprotective profile of pyridothiazepines with blocking activity of the mitochondrial Na(+)/Ca(2+) exchanger. Eur. J. Med. Chem. *109*, 114-123. 10.1016/j.ejmech.2015.12.043.

69. Viejo, L., Rubio-Alarcon, M., Arribas, R.L., Moreno-Castro, M., Perez-Marin, R., Braun-Cornejo, M., Estrada-Valencia, M., and de Los Rios, C. (2021). Synthesis and Biological Assessment of 4,1-Benzothiazepines with Neuroprotective Activity on the Ca(2+) Overload for the Treatment of Neurodegenerative Diseases and Stroke. Molecules *26*. 10.3390/molecules26154473.

70. Liew, S.S., Qin, X., Zhou, J., Li, L., Huang, W., and Yao, S.Q. (2021). Smart Design of Nanomaterials for Mitochondria-Targeted Nanotherapeutics. Angew. Chem. Int. Ed. Engl. *60*, 2232-2256. 10.1002/anie.201915826.

71. Jobin, K., Muller, D.N., Jantsch, J., and Kurts, C. (2021). Sodium and its manifold impact on our immune system. Trends Immunol. *42*, 469-479. 10.1016/j.it.2021.04.002.

72. Thowsen, I.M., Karlsen, T.V., Nikpey, E., Haslene-Hox, H., Skogstrand, T., Randolph, G.J., Zinselmeyer, B.H., Tenstad, O., and Wiig, H. (2022). Na(+) is shifted from the extracellular to the intracellular compartment and is not inactivated by glycosaminoglycans during high salt conditions in rats. J. Physiol. *600*, 2293-2309. 10.1113/JP282715.

73. Farh, K.K., Marson, A., Zhu, J., Kleinewietfeld, M., Housley, W.J., Beik, S., Shoresh, N., Whitton, H., Ryan, R.J., Shishkin, A.A., et al. (2015). Genetic and epigenetic fine mapping of causal autoimmune disease variants. Nature *518*, 337-343. 10.1038/nature13835.

74. Subramanian, A., Tamayo, P., Mootha, V.K., Mukherjee, S., Ebert, B.L., Gillette, M.A., Paulovich, A., Pomeroy, S.L., Golub, T.R., Lander, E.S., and Mesirov, J.P. (2005). Gene set enrichment analysis: a knowledge-based approach for interpreting genome-wide expression profiles. Proc. Natl. Acad. Sci. U. S. A. *102*, 15545-15550. 10.1073/pnas.0506580102.

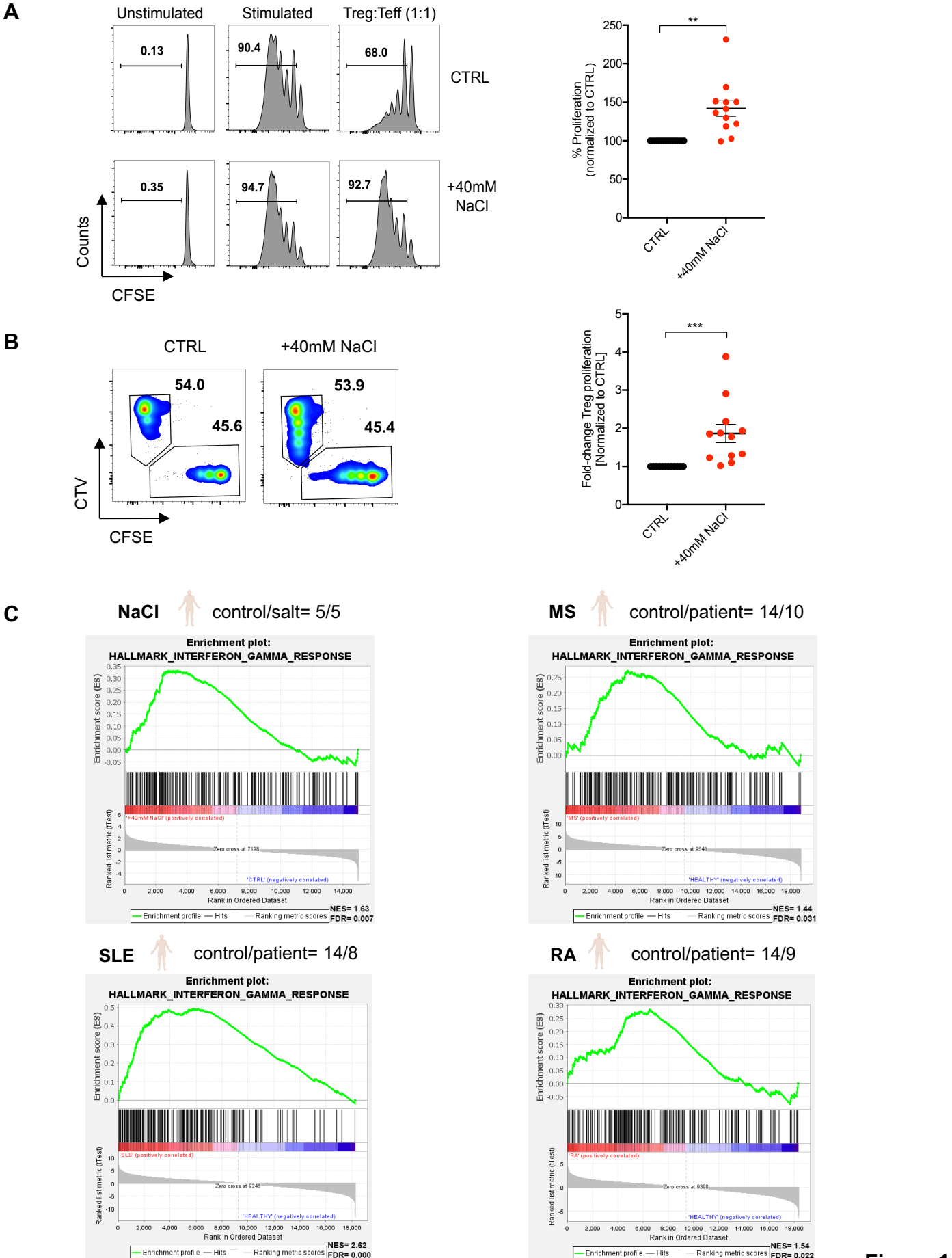
A
Unstimulated
Stimulated
Treg:Teff (1:1)
0.13
90.4
68.0
CTRL
0.35
94.7
92.7
+40mM NaCl
Counts
CFSE
% Proliferation (normalized to CTRL)
**
CTRL
+40mM NaCl
B
CTRL
+40mM NaCl
54.0
45.6
53.9
45.4
CTV
CFSE
Fold-change Treg proliferation [Normalized to CTRL]
***
CTRL
+40mM NaCl
C
NaCl
control/salt= 5/5
Enrichment plot:
HALLMARK_INTERFERON_GAMMA_RESPONSE
Enrichment score (ES)
'+40mM NaCl' (positively correlated)
Ranked list metric (fTest)
Zero cross at 7198
'CTRL' (negatively correlated)
Rank in Ordered Dataset
Enrichment profile
Hits
Ranking metric scores
NES= 1.63
FDR= 0.007
MS
control/patient= 14/10
Enrichment plot:
HALLMARK_INTERFERON_GAMMA_RESPONSE
Enrichment score (ES)
'MS' (positively correlated)
Ranked list metric (fTest)
Zero cross at 9541
'HEALTHY' (negatively correlated)
Rank in Ordered Dataset
Enrichment profile
Hits
Ranking metric scores
NES= 1.44
FDR= 0.031
SLE
control/patient= 14/8
Enrichment plot:
HALLMARK_INTERFERON_GAMMA_RESPONSE
Enrichment score (ES)
'SLE' (positively correlated)
Ranked list metric (fTest)
Zero cross at 9246
'HEALTHY' (negatively correlated)
Rank in Ordered Dataset
Enrichment profile
Hits
Ranking metric scores
NES= 2.62
FDR= 0.000
RA
control/patient= 14/9
Enrichment plot:
HALLMARK_INTERFERON_GAMMA_RESPONSE
Enrichment score (ES)
'RA' (positively correlated)
Ranked list metric (fTest)
Zero cross at 9398
'HEALTHY' (negatively correlated)
Rank in Ordered Dataset
Enrichment profile
Hits
Ranking metric scores
NES= 1.54
FDR= 0.022

Figure 1

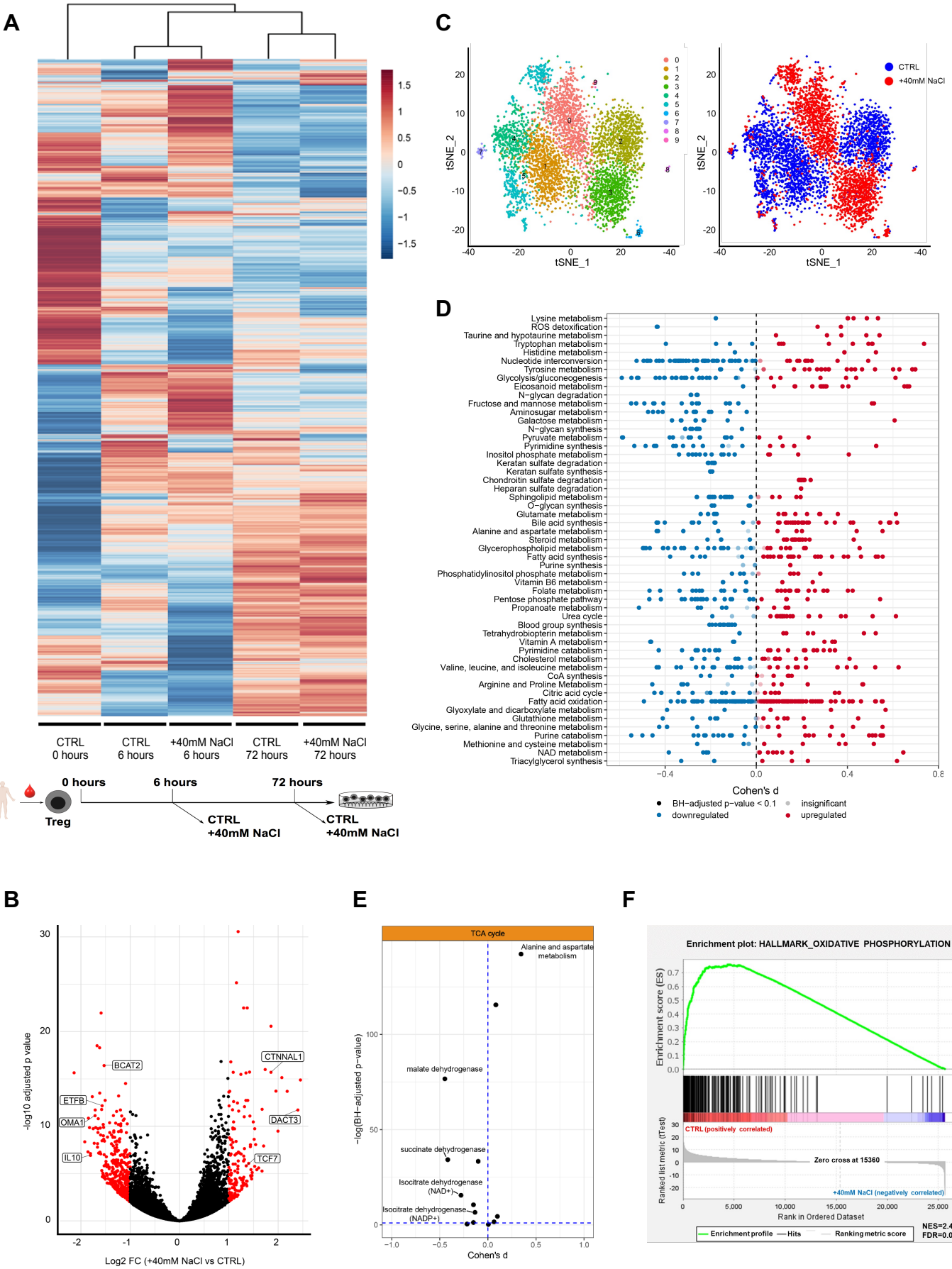
A
1.5
1
0.5
0
−0.5
−1
−1.5
CTRL 0 hours
CTRL 6 hours
+40mM NaCl 6 hours
CTRL 72 hours
+40mM NaCl 72 hours
0 hours
6 hours
72 hours
Treg
CTRL +40mM NaCl
CTRL +40mM NaCl
C
tSNE_2
tSNE_1
CTRL
+40mM NaCl
D
Lysine metabolism
ROS detoxification
Taurine and hypotaurine metabolism
Tryptophan metabolism
Histidine metabolism
Nucleotide interconversion
Tyrosine metabolism
Glycolysis/gluconeogenesis
Eicosanoid metabolism
N−glycan degradation
Fructose and mannose metabolism
Aminosugar metabolism
Galactose metabolism
N−glycan synthesis
Pyruvate metabolism
Pyrimidine synthesis
Inositol phosphate metabolism
Keratan sulfate degradation
Keratan sulfate synthesis
Chondroitin sulfate degradation
Heparan sulfate degradation
Sphingolipid metabolism
O−glycan synthesis
Glutamate metabolism
Bile acid synthesis
Alanine and aspartate metabolism
Steroid metabolism
Glycerophospholipid metabolism
Fatty acid synthesis
Purine synthesis
Phosphatidylinositol phosphate metabolism
Vitamin B6 metabolism
Folate metabolism
Pentose phosphate pathway
Propanoate metabolism
Urea cycle
Blood group synthesis
Tetrahydrobiopterin metabolism
Vitamin A metabolism
Pyrimidine catabolism
Cholesterol metabolism
Valine, leucine, and isoleucine metabolism
CoA synthesis
Arginine and Proline Metabolism
Citric acid cycle
Fatty acid oxidation
Glyoxylate and dicarboxylate metabolism
Glutathione metabolism
Glycine, serine, alanine and threonine metabolism
Purine catabolism
Methionine and cysteine metabolism
NAD metabolism
Triacylglycerol synthesis
Cohen's d
BH−adjusted p−value < 0.1
insignificant
downregulated
upregulated
B
-log10 adjusted p value
Log2 FC (+40mM NaCl vs CTRL)
BCAT2
CTNNAL1
ETFB
OMA1
DACT3
IL10
TCF7
E
TCA cycle
Alanine and aspartate metabolism
malate dehydrogenase
succinate dehydrogenase
Isocitrate dehydrogenase (NAD+)
Isocitrate dehydrogenase (NADP+)
−log(BH−adjusted p−value)
Cohen's d
F
Enrichment plot: HALLMARK_OXIDATIVE_PHOSPHORYLATION
Enrichment score (ES)
CTRL (positively correlated)
Zero cross at 15360
+40mM NaCl (negatively correlated)
Ranked list metric (Test)
Rank in Ordered Dataset
Enrichment profile
Hits
Ranking metric score
NES=2.4
FDR=0.001

Figure 2

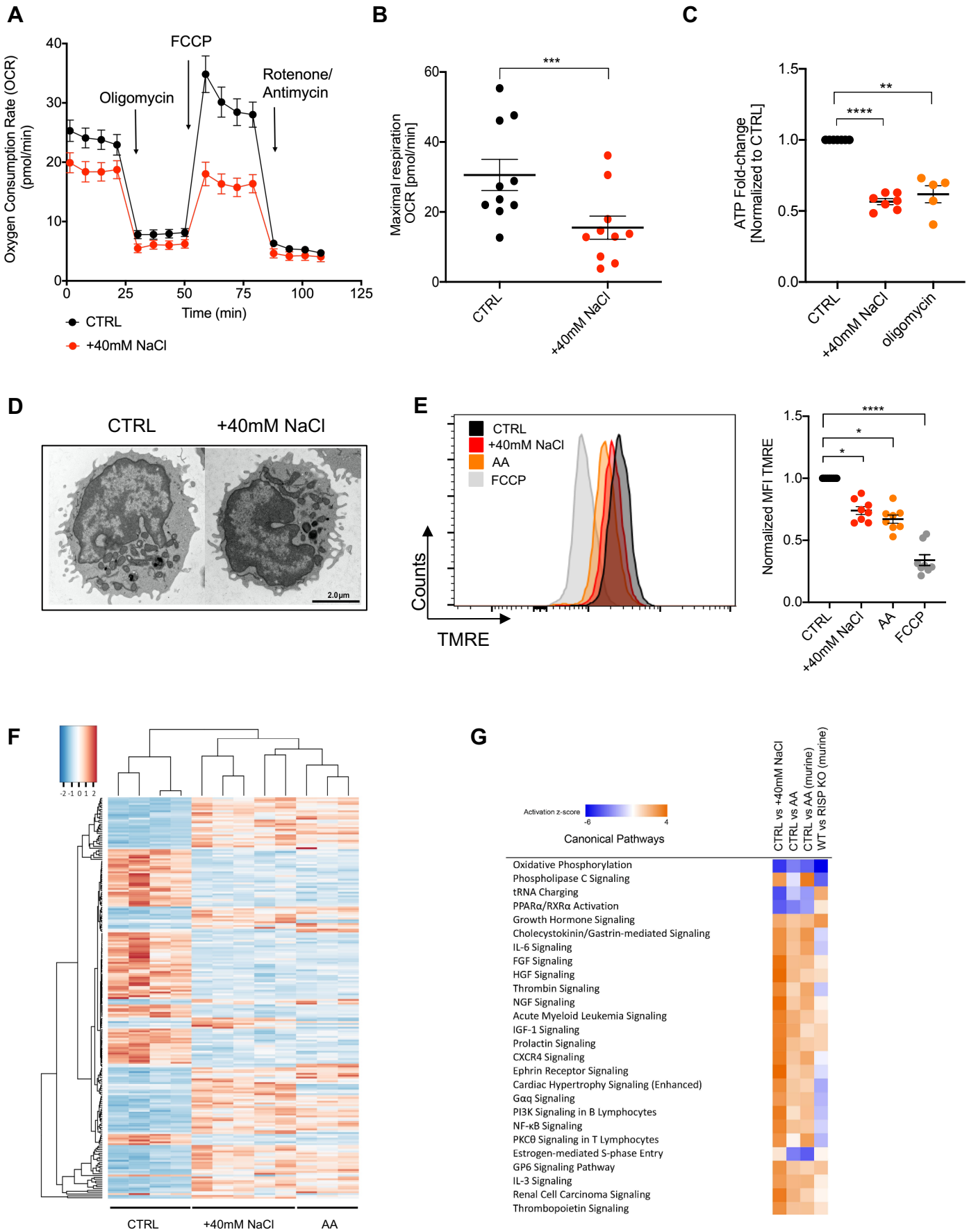
A
Oxygen Consumption Rate (OCR) (pmol/min)
Oligomycin
FCCP
Rotenone/ Antimycin
Time (min)
CTRL
+40mM NaCl
B
Maximal respiration OCR [pmol/min]
***
CTRL
+40mM NaCl
C
ATP Fold-change [Normalized to CTRL]
**
****
CTRL
+40mM NaCl
oligomycin
D
CTRL
+40mM NaCl
2.0µm
E
CTRL
+40mM NaCl
AA
FCCP
Counts
TMRE
Normalized MFI TMRE
****
*
*
CTRL
+40mM NaCl
AA
FCCP
F
CTRL
+40mM NaCl
AA
G
Activation z-score
Canonical Pathways
CTRL vs +40mM NaCl
CTRL vs AA
CTRL vs AA (murine)
WT vs RISP KO (murine)
Oxidative Phosphorylation
Phospholipase C Signaling
tRNA Charging
PPARα/RXRα Activation
Growth Hormone Signaling
Cholecystokinin/Gastrin-mediated Signaling
IL-6 Signaling
FGF Signaling
HGF Signaling
Thrombin Signaling
NGF Signaling
Acute Myeloid Leukemia Signaling
IGF-1 Signaling
Prolactin Signaling
CXCR4 Signaling
Ephrin Receptor Signaling
Cardiac Hypertrophy Signaling (Enhanced)
Gαq Signaling
PI3K Signaling in B Lymphocytes
NF-κB Signaling
PKCθ Signaling in T Lymphocytes
Estrogen-mediated S-phase Entry
GP6 Signaling Pathway
IL-3 Signaling
Renal Cell Carcinoma Signaling
Thrombopoietin Signaling

Figure 3

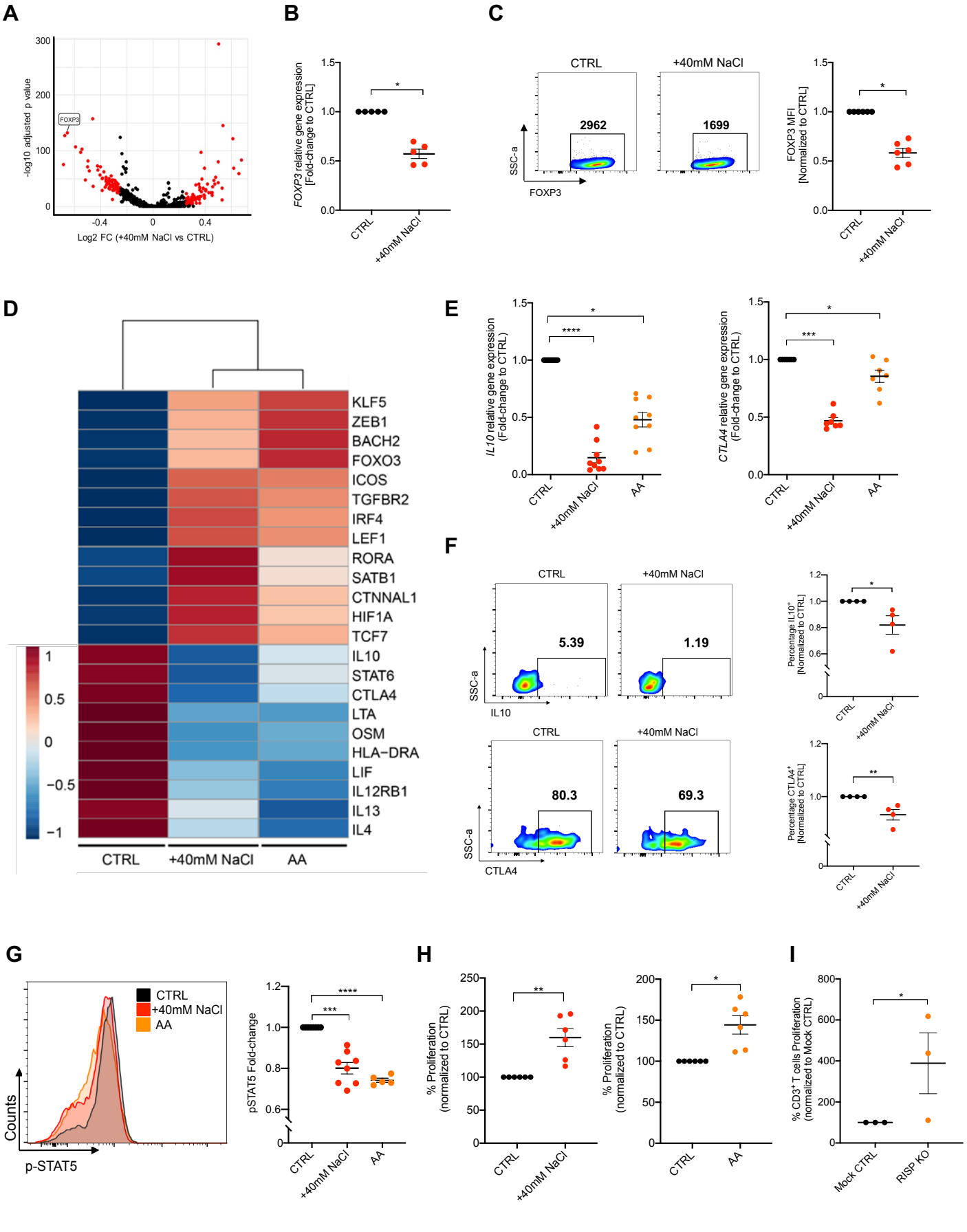
A
-log10 adjusted p value
Log2 FC (+40mM NaCl vs CTRL)
FOXP3
B
FOXP3 relative gene expression [Fold-change to CTRL]
CTRL
+40mM NaCl
C
CTRL
+40mM NaCl
2962
1699
SSC-a
FOXP3
FOXP3 MFI [Normalized to CTRL]
D
KLF5
ZEB1
BACH2
FOXO3
ICOS
TGFBR2
IRF4
LEF1
RORA
SATB1
CTNNAL1
HIF1A
TCF7
IL10
STAT6
CTLA4
LTA
OSM
HLA-DRA
LIF
IL12RB1
IL13
IL4
CTRL
+40mM NaCl
AA
E
IL10 relative gene expression (Fold-change to CTRL)
CTLA4 relative gene expression (Fold-change to CTRL)
F
5.39
1.19
80.3
69.3
IL10
CTLA4
Percentage IL10+ [Normalized to CTRL]
Percentage CTLA4+ [Normalized to CTRL]
G
CTRL
+40mM NaCl
AA
Counts
p-STAT5
pSTAT5 Fold-change
H
% Proliferation (normalized to CTRL)
I
% CD3+ T cells Proliferation (normalized to Mock CTRL)
Mock CTRL
RISP KO

Figure 4

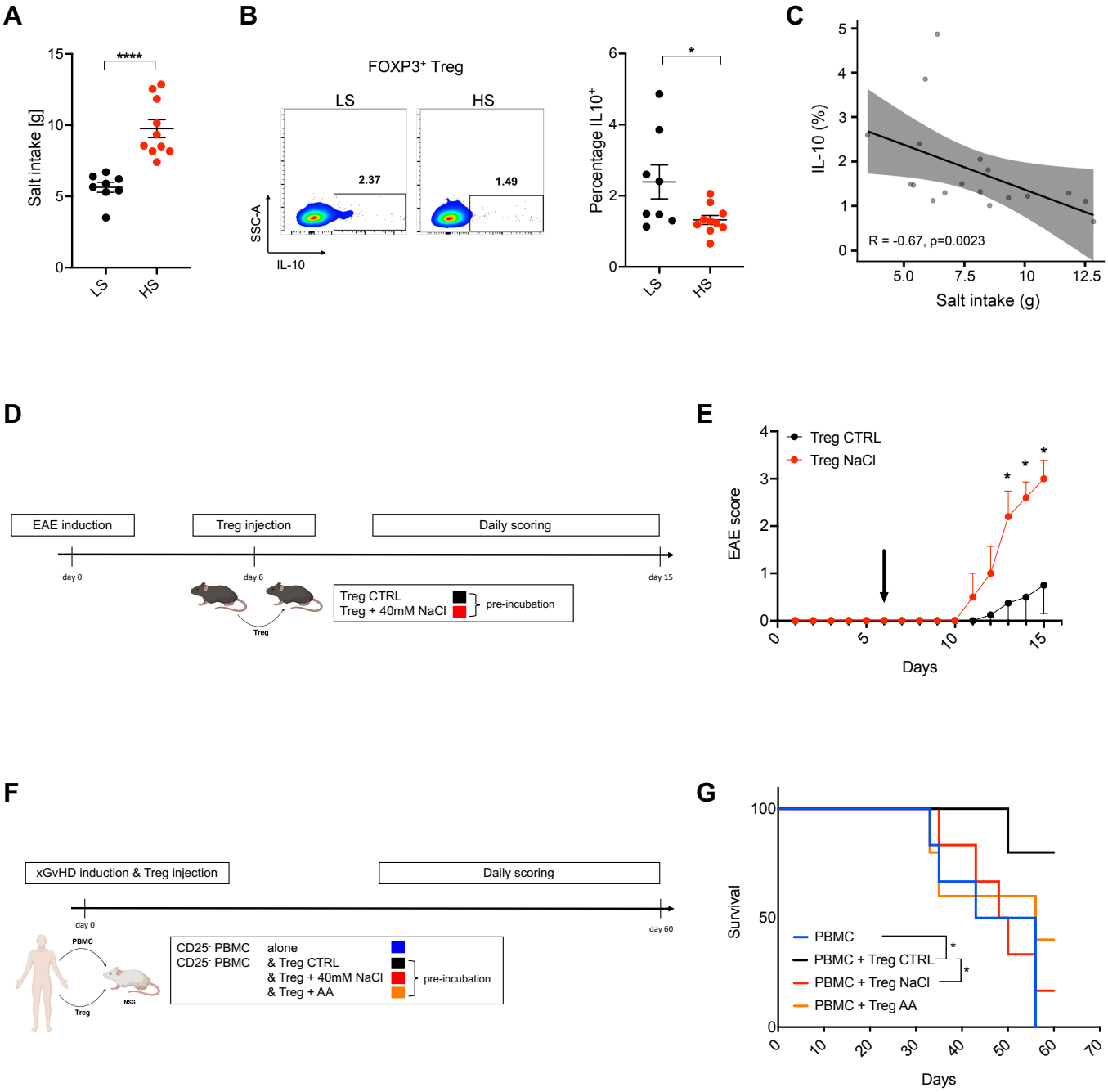
A
Salt intake [g]
****
LS
HS
B
FOXP3⁺ Treg
LS
HS
2.37
1.49
SSC-A
IL-10
Percentage IL10⁺
*
C
IL-10 (%)
R = -0.67, p=0.0023
Salt intake (g)
D
EAE induction
Treg injection
Daily scoring
day 0
day 6
day 15
Treg
Treg CTRL
Treg + 40mM NaCl
pre-incubation
E
Treg CTRL
Treg NaCl
EAE score
Days
F
xGvHD induction & Treg injection
Daily scoring
day 0
day 60
PBMC
Treg
NSG
CD25⁻ PBMC
CD25⁻ PBMC
alone
& Treg CTRL
& Treg + 40mM NaCl
& Treg + AA
pre-incubation
G
Survival
PBMC
PBMC + Treg CTRL
PBMC + Treg NaCl
PBMC + Treg AA
Days

Figure 5

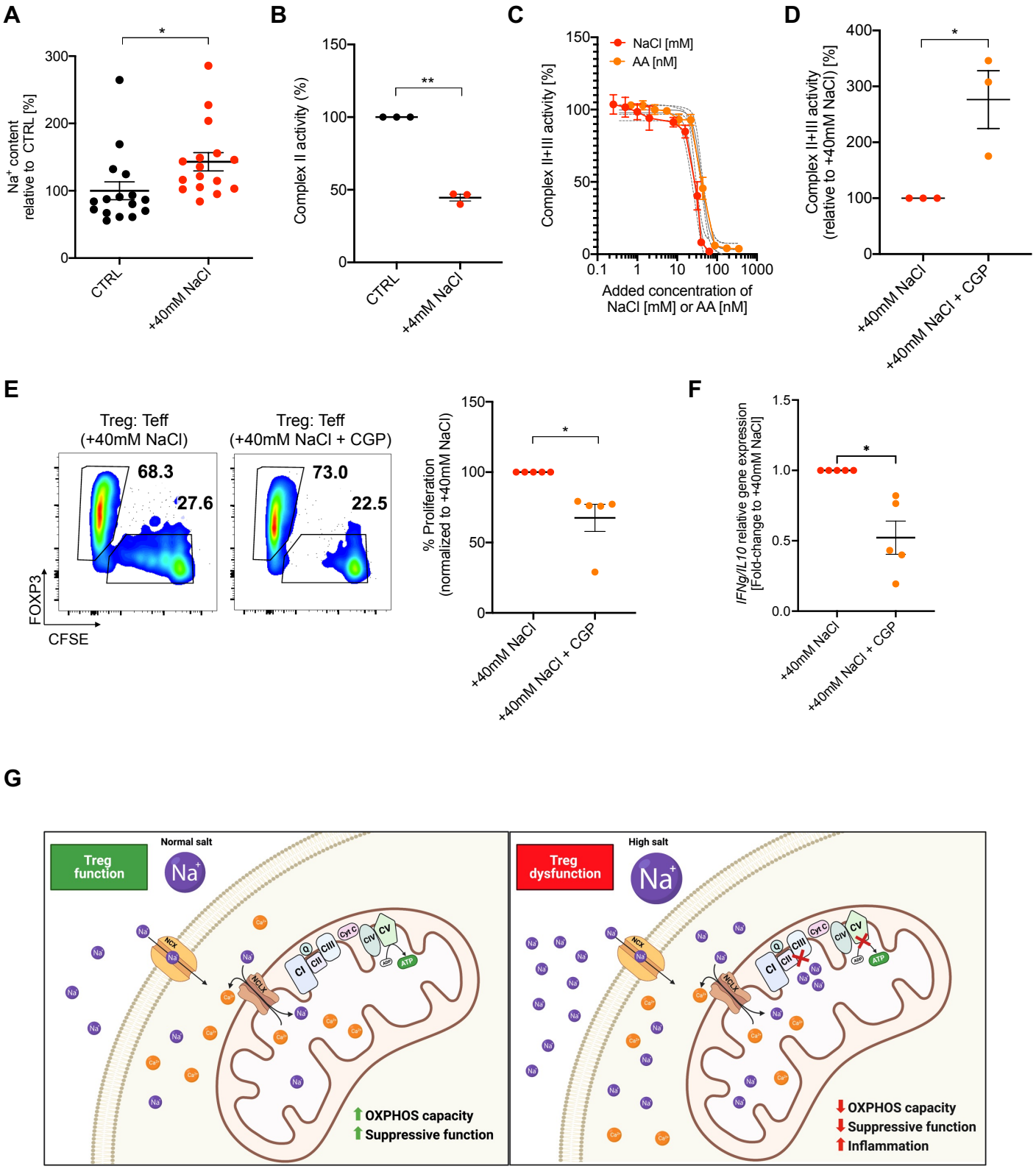
A
Na+ content relative to CTRL [%]
CTRL
+40mM NaCl
B
Complex II activity (%)
CTRL
+4mM NaCl
C
NaCl [mM]
AA [nM]
Complex II+III activity [%]
Added concentration of NaCl [mM] or AA [nM]
D
Complex II+III activity (relative to +40mM NaCl) [%]
+40mM NaCl
+40mM NaCl + CGP
E
Treg: Teff (+40mM NaCl)
Treg: Teff (+40mM NaCl + CGP)
68.3
27.6
73.0
22.5
FOXP3
CFSE
% Proliferation (normalized to +40mM NaCl)
+40mM NaCl
+40mM NaCl + CGP
F
IFNg/IL10 relative gene expression [Fold-change to +40mM NaCl]
+40mM NaCl
+40mM NaCl + CGP
G
Treg function
Normal salt
Na+
OXPHOS capacity
Suppressive function
Treg dysfunction
High salt
Na+
OXPHOS capacity
Suppressive function
Inflammation

Figure 6